universität wien

MASTERARBEIT / MASTER'S THESIS

Titel der Masterarbeit / Title of the Master's Thesis

„Characterization of a high power Yb-based mode-locked laser“

verfasst von / submitted by

Michael Leskowschek, BSc

angestrebter akademischer Grad / in partial fulfilment of the requirements for the degree of

Master of Science (MSc)

Wien, 2022 / Vienna, 2022

Studienkennzahl lt. Studienblatt / degree programme code as it appears on the student record sheet:	UA 066 876
Studienrichtung lt. Studienblatt / degree programme as it appears on the student record sheet:	Masterstudium Physik
Betreut von / Supervisor:	Ass.-Prof. Dipl.-Phys. Dr. Oliver H. Heckl

Contents

Acknowledgements

After 7 years the journey comes to an end. It was not always easy, but I got through it by the help of some very important people. This chapter is dedicated to all those people, without whom I would not have done it.

First of all I want to thank Dr. Oliver H. Heckl, for igniting my interest in photonics, with his lecture. Furthermore, I want to thank you for letting me join your group and giving me the chance to write my Master's thesis.
Another big thank you goes to Dr. Valentina Shumakova, for teaching me so many things in the laboratory and supporting me in writing my thesis. Thank you for all your efforts and the time you have spent improving my writing style.
At this point, I also want to particularly thank Vito Pecile for introducing me to the laboratory and experimental world of lasers. Thank you for all the support you showed me and all the nice discussions we had, no matter if they were related to physics or to personal issues.
Many thanks go to the whole CDL for mid-IR spectroscopy and semiconductor optics group, for being the best colleagues one can wish for. Thank you for making troubling laboratory or office days funny again and helping everyone out where you can.

A very special thank you is denoted to my family, my parents Ruth and Heinrich and my brother Daniel. Thank you for supporting me emotionally when I doubted myself and supporting me in all the decisions I made. But most importantly, thank you for your financial support. Otherwise I would not be able to write those lines of text right now.
Outside the experimental work and hard work for my thesis, there are a lot of people who joined me on my way, some for a longer part and some for just some months. The list of friends who made studying do much fun and stuck with me through exercise courses and exams is too long to be named here and it will cost me more than one beer to thank you all.
Out of this group I want to highlight especially one person who (involuntarily) stuck to me starting from day one. Dear Max thank you for all the great years we had and cheers to many more to come. I will never forget the first evening at the Pub with the triangle of consumption. Without you wide parts of my studies would not have been possible and definitely it would not have been so much fun.

Last and most of all I want to thank my girlfriend Sarah. You have always been there for me and supported me through all the hard times starting even way before going to Vienna. Thank you for having my back no matter what obstacles were in my way and thank you even more for kicking my butt when I most needed it.

Chapter 1

Introduction

Applications like remote sensing [5], ranging [12], chemical analysis in health and environmental sciences [58], and spectroscopy of extraterrestrial objects need precise spectroscopic databases in order to perform high-quality measurements. The mid-IR wavelength range (2.5 - 20 μm) is of special interest since here fundamental molecular vibrational transitions take place. However, acquiring high precision line positions and broadening coefficients in this spectral region is challenging, and subject of ongoing research [14]. One obstacle, to perform exact data acquisition, is the Doppler broadening related to molecular motion. There are several ways to measure Doppler-free transition linewidths and position [10, 6, 7]. However, those methods, relying on cooling or optically trapping the molecules, require high-cost setups and, lack the possibility to investigate hot-band transitions [46]. Alternatively, one can apply saturation, or Lamb-dip, spectroscopy. This method relies on depleting the ground state of the transitions of interest. For those purposes Lamb-dip spectroscopy needs a high-power light source in the mid-IR. Moreover, since typical linewidths of Doppler-fee transitions are in the region of kHz, which is much narrower than common transition bandwidths in the region from 10 MHz to 1 GHz, this light source is required to have high spectral resolution and stability.

This work will therefore present a roadmap to establish a suitable light source in the mid-IR, to perform precision spectroscopy. To produce the light source optical parametric conversion will be used, due to the absence of broadband, high-power, and, in a wide range, tuneable laser materials in the mid-IR [3]. Since the nonlinear effects, driving the parametric processes, have low a conversion efficiency high peak and average powers of the pump laser are required. Therefore, the design and development of a suitable pump laser system is the first step. In this thesis, I will present the design guidelines, implementation, and characterisation of a high peak and average power near infrared (near-IR) laser system, which can be used as a pump laser for a mid-IR source used in precision spectroscopy.

The generation of broadband laser pulses with high peak and average power is generally not a trivial task. First, the high intensities of the amplified laser pulses lead to the accumulation of the nonlinear phase, spectral and temporal distortions, and can eventually damage optical elements [61]. Secondly, laser amplification has a high thermal load, as a result of the quantum defect of the used gain material, non-emitting transitions, and parasitic absorptions [59]. The heat can lead to thermal lensing effects, destruction of optical elements, mechanical stress, and detuning of opto-mechanics, which can lead to a beam walk-off. Finally, the generation of broadband ultrashort pulses can be disrupted by gain narrowing or the amplification of spontaneously emitted photons [49].

There are many options for generating a feasible laser system. Among them, Ytterbium (Yb) -doped fiber lasers are attractive for generating high peak and average power fs pulses. Thermal management in fibers is easily applicable, since the fibers have a large ratio of surface to volume [31]. Additionally, using Yb as a gain material provides a small quantum defect further easing thermal management. With the help of large mode are (LMA) and photonic crystal fibers (PCFs) nonlinearities in the system can be reduced by spatially broadening the light pulses [21, 26]. Additionally, CPA can be used to temporally spread the pulse, thus further reducing the intensity [47]. Yb, used as the active medium, supports broad amplification bandwidth and enables sub-100 fs pulses [21]. Moreover, the components for building an Yb:fiber-based CPA are easily available and relatively cheap, thus allowing for tailoring the performance of the system to the required needs [21]. In chapter 2.2.2 the principles of dispersion management, needed to perform CPA, are presented. The details for laser amplification are given in chapter 2.2.3. Chapter 4 deals with the design and performance of the CPA system.

Besides the high peak and average powers, high repetition rates, and short pulse duration the system needs to provide high spectral resolution. A widely known and elegant solution to obtain necessary precision for spectroscopy is by using an OFC. An OFC consists of narrow and equally spaced frequency lines [40]. The resolution of the individual comb teeth is defined by the stability of the laser system and by the properties of amplitude and phase noise of the OFC. Those noise sources can originate from several sources like thermal drifts, mechanical or acoustic vibrations, quantum noise or nonlinear effects and must be taken into account when designing the laser system [38, 39].

There are several options to produce an OFC. One of them is, to use a stabilized mode-locked (ML) laser oscillator. To realize a ML-oscillator the same Yb:fiber medium can be used as discussed before. This design yields not only excellent noise properties, but also provides a robust, reliable, and versatile laser design. However, the average output power resulting from this laser is usually limited by tens of mW, and therefore not sufficient to be applied for parametric conversion and subsequent precision spectroscopy [31, 21]. Chapter 2.1, gives a detailed description on OFCs and noise in OFCs as well as a discussion of noise sources in OFCs.

The aim of this thesis is dedicated to describing the development as well as the characterization of a low noise, high power Yb based amplifier system. We use a homebuilt figure-9-laser providing narrow comb linewidths. The produced OFC is amplified in a three stage CPA system to 100 W of average power. The presented system preserves the low noise properties of the seed laser. We show that the amplitude noise is limited by the one of the pump diode, which is the lowest possible noise level. The system achieves a beam quality of $M_x^2 = 1.05$ and $M_y^2 = 1.22$ after compression. The compressed pulses have a pulse duration of 230 fs and a spectral bandwidth of 10 nm, optimized to the requirements for optical parametric conversion.

Chapter 2

Theory

2.1 Frequency Combs

Laser light is generated in a laser cavity, which has two end mirrors and a pumped gain medium. The light, going back and forth in the resonator cavity, is represented by a superposition of electro-magnetic (EM) waves. These EM waves have no fixed phase relationship and therefore interfere randomly with each other. Their frequency difference is given by the length of the laser cavity L [53, 11]:

$$\delta\nu = \frac{c}{2L} \tag{2.1}$$

where $\Delta\nu$ is the frequency difference given between two EM waves and c denotes the speed of light. To produce a pulsed laser the EM waves need to have a fixed phase relationship, such that they interfere constructively and form a standing wave inside the resonator cavity. Since the EM waves are also called resonator modes, one speaks of locking the phase of the modes to each other, thus also called ML [11].

To introduce ML, the losses inside the cavity are getting modulated, such that the EM waves in the cavity are brought to a fixed phase relationship. There are two fundamental ML ways, active and passive ML. While active ML generates the losses through an external device, like an acousto-optic-modulator (AOM) or an electro-optic modulator (EOM), passive ML can be achieved by implementing a saturable absorber [53].

In the time domain a pulse train is generated when ML a laser. The separation between the pulses is set by the roundtrip time T_{R}, the EM waves take for one roundtrip inside the cavity [48] [53]. In frequency domain, this separation corresponds to the repetition rate f_{rep}, which is inversely proportional to T_{R}:

$$f_{\mathrm{rep}} = \frac{1}{T_{\mathrm{R}}}$$

The electric field $E(t)$ of the pulse train is described by a single pulse convoluted with an infinite series of delta functions:

$$E(t) = a(t)\mathrm{e}^{(\mathrm{i}\omega_c t + \mathrm{i}\omega_{\mathrm{offset}} t)} \sum_{\mathrm{m}=-\infty}^{\infty} \delta(t - \mathrm{m}T_{\mathrm{R}}) \tag{2.2}$$

Here the single pulse is given by the amplitude of the electric field $A(t)$ multiplied by its phase (ω_c - ω_{offset}). The infinite series of delta functions is given by the sum of the different modes m inside the cavity. The offset frequency describes a slip of the phase (carrier) in comparison to the amplitude (or envelope of the pulse) at each roundtrip in the cavity, and therefore for each produced pulse. Therefore, it is called carrier envelope offset (CEO) [15]:

$$f_{\text{CEO}} = \frac{\omega_{\text{CEO}}}{2\pi} = \frac{\Delta\phi_{\text{CEO}}}{2\pi T_{\text{R}}} = \frac{\Delta\phi_{\text{CEO}}}{2\pi}\text{mod}2\pi f_{\text{rep}} \tag{2.3}$$

Performing a Fourier transformation on equation 2.2, representing the pulse train in time domain, leads to the representation in the frequency domain:

$$\tilde{E}(\omega) = \tilde{a}(\omega - \omega_c)\frac{1}{2\pi}\sum_{\text{m}=-\infty}^{\infty}\delta(\omega - \text{m}2\pi f_{\text{rep}} - 2\pi f_{\text{CEO}}) \tag{2.4}$$

Considering the principal frequencies (f_{CEO} and f_{rep}), an individual comb line, with the mode number n, can be described by: [15]:

$$f_{\text{n}} = f_{\text{CEO}} + \text{n}f_{\text{rep}} \tag{2.5}$$

Where f_{rep} is the repetition rate of the laser assigning the individual comb spacing, n is a natural number, denoting the mode number, and f_{CEO} is the CEO frequency. In other words, the OFC is a pulsed laser consisting of discrete frequency lines [40], which are equally spaced by the repetition rate f_{rep} of the laser.

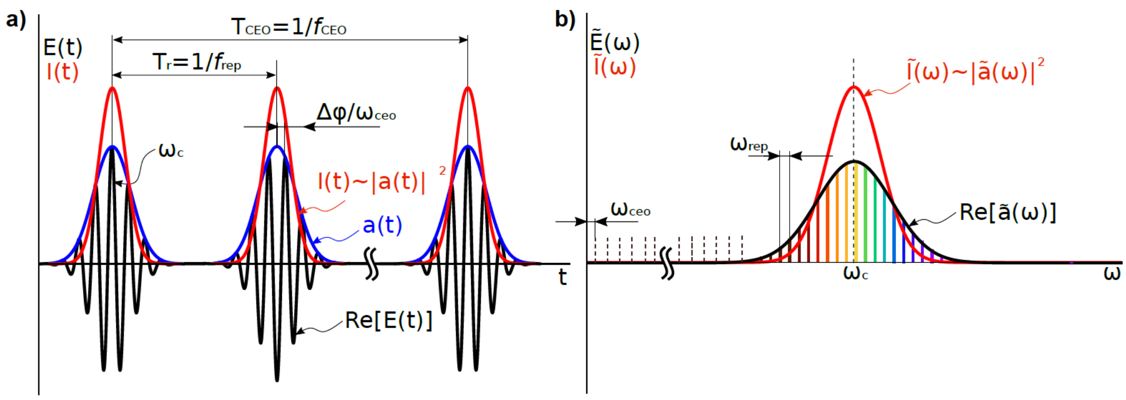

Figure 2.1: The representation of an frequency comb a) in form of an infinite pulse train, in the time domain, is shown. b) shows the representation of the OFC in the frequency domain. In this figure $\omega_{\text{CEO}} = 2\pi f_{\text{CEO}}$ and $\omega_{\text{rep}} = 2\pi f_{\text{rep}}$. Reprinted with permission from Jakob Fellinger [11].

2.1.1 Noise in Frequency Combs

The pulse train produced by an ideal OFC, as given by the equations 2.4 and 2.2 can also be described in terms of intensity $I(t)$, in form of a convolution of the pulse energy ($E_{\text{Pulse}} = P_{\text{av}}T_{\text{R}}$) with discrete delta lines. This approximation is possible, since the roundtrip time is much shorter than the duration of the individual pulses [30]:

$$I(t) = P_{\text{av}}T_{\text{R}}\sum_{\text{n}=-\infty}^{\infty}\delta(t - \text{n}T_{\text{R}}) \tag{2.6}$$

Here, P_{av} is the average power. The corresponding representation in the frequency domain is called the power spectral density (PSD) $S(f)$:

$$S(f) = P_{\text{av}}^2\sum_{\text{n}=-\infty}^{\infty}\delta(f - \text{n}f_{\text{rep}}) \tag{2.7}$$

In reality a laser exhibits fluctuations of its output power and optical phase, due to various reasons. The two fundamental noise characteristics, a pulsed laser can exhibit, are the PN and relative intensity noise (RIN), described in detail below.

Relative Intensity Noise

The RIN, or in other words amplitude noise, describes a fluctuation of the lasers output power. Typically, it is described by the power level of the laser noise, normalized to its average power. A laser exhibiting RIN, compared to an ideal laser, exhibits a random power fluctuation $N(t)$ at every rountrip in the cavity. [30].

$$I(t) = P_{\text{av}} T_{\text{R}} (1 + N(t)) \sum_{\text{n}=-\infty}^{\infty} \delta(t - \text{n}T_{\text{R}}) \tag{2.8}$$

Accordingly, in the frequency domain fluctuations $\tilde{N}(f)$, as the Fourier transform of $N(t)$, are added [30]:

$$S(f) = P_{\text{av}}^2 \sum \text{n} = -\infty^{\infty} \delta(f - \text{n}f_{\text{rep}}) + (N(f - \text{n}f_{\text{rep}}))^2 \tag{2.9}$$

Due to the quadratic dependence on the difference in frequency, sidebands are added to the delta functions [30]. A representation of the RIN in both, time and frequency domain, can be seen in figure 4.15.

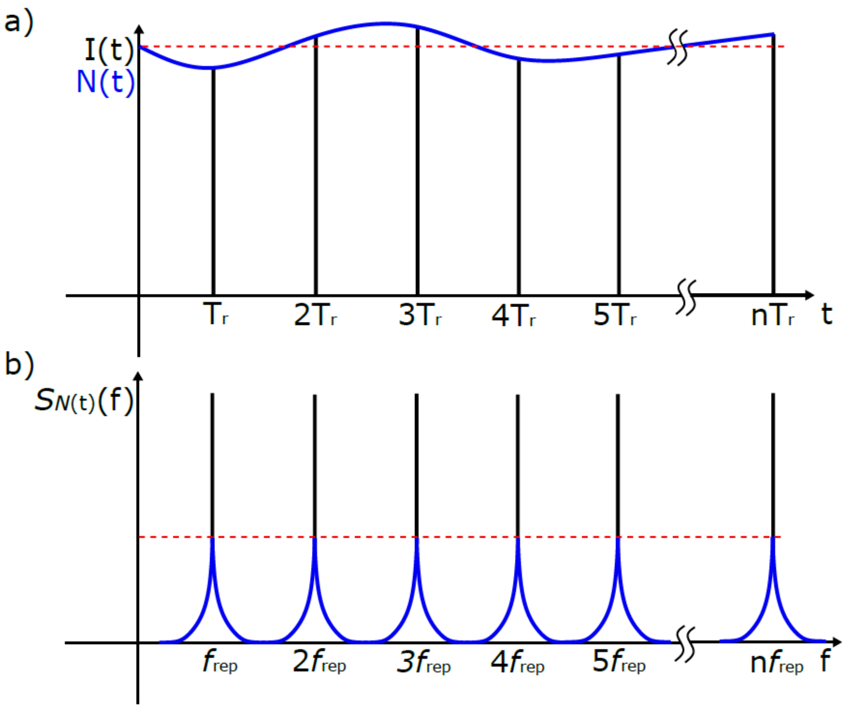

Figure 2.2: a) The power fluctuation of every pulse in time domain; b) In frequency domain with sidebands on the different repetition rates. Reprinted with permission from Jakob Fellinger [11].

Phase Noise

The second fundamental kind of noise denotes a fluctuation of the optical phase, or timing jitter, between the pulses. This creates a slightly aperiodic signal. In the time domain this means that the arrival time of the pulse on, for instance, a photo detector varies by a factor of $\Delta T_{\text{R(t)}}$ with respect to their ideal arrival time T_{R} [41]. The modified intensity of the pulse train is therefore[30]:

$$I_{\Delta T_{\text{R}(t)}} = P_{\text{av}} T_{\text{R}} \sum_{\text{n}=-\infty}^{\infty} \delta(t - \text{n}T_{\text{R}} - \Delta T_{\text{R}(t)}) \tag{2.10}$$

Since $\Delta T_{\mathrm{R}(t)}$ is much smaller than T_{R} the Fourier shifting theorem can be used to represent the consequences in the frequency domain PSD [30]:

$$S(f) = P_{\mathrm{av}}^2 \sum \mathrm{n} = -\infty^{\infty} \delta(f - n f_{\mathrm{rep}}) + n^2 4\pi^2 f_{\mathrm{rep}}^2 [\Delta\tilde{T}(f - \mathrm{n} f_{\mathrm{rep}})]^2) \tag{2.11}$$

In frequency domain the phase noise depends quadratically on the mode order n and the repetition frequency, leading to sidebands increasing by a factor n^2. The PN is caused by so called quantum noise [30].

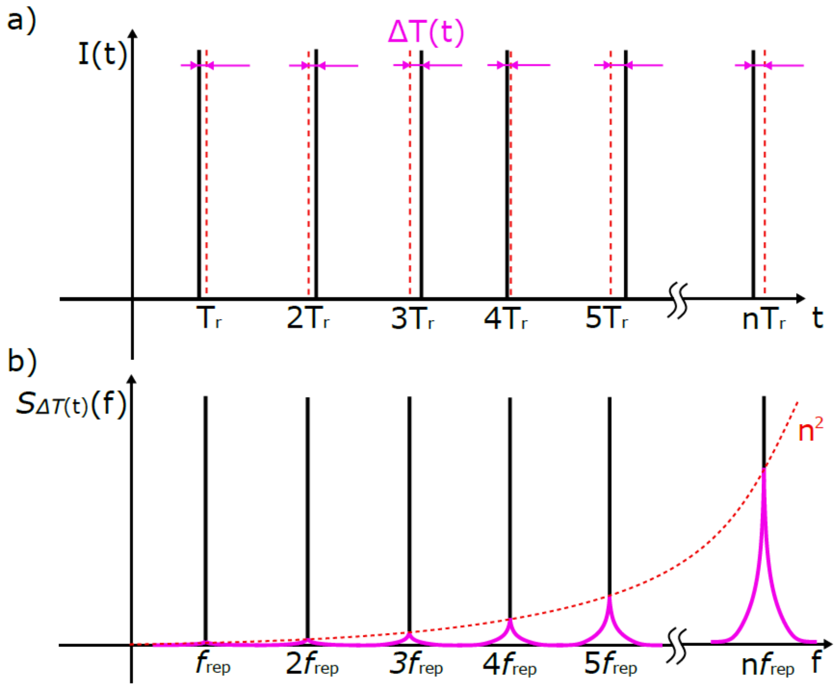

Figure 2.3: a) Shows the consequence of PN in time domain ($I(t)$); b) shows the consequences in frequency domain. In correspondence to equation 2.11 a quadratic dependence n^2 of the noise with the repetition rate is depicted. Reprinted with permission from Jakob Fellinger [11].

Noise Sources in Laser Systems

The previously described PN and RIN are fundamental noise properties, which laser can experience. Those noise properties have various sources of origin like mechanical, electrical or quantum noise [36]. PN is mainly influenced by quantum noise, whereas RIN can have additional origins like mechanical or electrical noise sources [38, 39, 30].
An amplifier system can be depicted as an additional noise source. As for the seed laser, additional PN and RIN can be introduced by both technical and quantum sources. A prominent example is amplified spontaneous emission (ASE), which is seeded by the spontaneous emission process (luminescence) 2.2.3. The luminescent light is emitted in any possible direction including the propagation direction of the seed laser light. In the case of fiber amplifiers, especially operating below the lasing threshold, ASE can exceed the intensity of stimulated emission. As ASE is the amplification of spontaneously emitted photon, it is more present in quasi three level systems (like Yb) than for instance in 4 level systems [33].
When designing a laser system for precision spectroscopy, high attention is brought to realizing a low noise system. This begins with having a low noise seed oscillator and furthermore, conserving the low noise quantities of the seed laser. This can be done by various measures, like keeping it mechanically stable and perform thermal management. Another possibility, especially for fiber amplifiers, is the saturation of the gain medium by the seed light and staying in a linear

amplification regime [55]. Thus, the dominating part of the RIN is the pump source of the gain medium, whereas the seed properties will get suppressed [55].
For a deeper insight into noise sources and their influence on laser systems [38, 39, 30] is recommended.

2.2 Chirped Pulse Amplification

As mentioned before, to perform spectroscopy in the mid-IR, high peak and average powers of the OFC are needed. One of the state-of-the art procedures to amplify laser pulses is CPA. A brief description of CPA is given here, before talking intensively about the basic principles of the method in the following chapters.
If a short laser pulse propagates through an optical fiber or gain material its peak intensities can become very large. Thus, easily damaging or destroying the gain medium or fiber, when exceeding their damage threshold. In 1985 Strickland and Mourou published a method for amplifying short laser pulses in radar technology, which gained them the Nobel prize in 2018 [47]. This method, known as CPA, first stretches the pulses before amplification and subsequent compression take place. As described in the following sections this is done by dispersive elements. Due to the longer pulse duration, the peak intensity decreases. Following amplification, the pulse is re-compressed by propagating it through a dispersive element, for instance gratings or prisms, again. Figure 2.4 indicates this process.

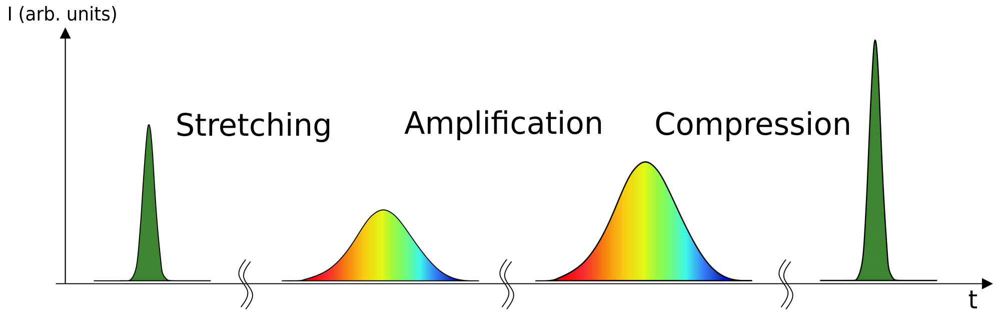

Figure 2.4: A schematic view of a light pulse undergoing CPA. The y-axis shows the intensity of the light pulse in arbitrary numbers. The x-axis denotes the propagation in time relative to the processes happening. As described, the initial light pulse (on the left) with too much intensity is stretched in order to decrease its peak intensities. Afterwards amplification takes place. In the end the pulse is re-compressed again.

There are several techniques to stretch and compress laser pulses. The methods can rely on material dispersion, mode dispersion in fibers, or by angular dispersion, resulting in an optical path length difference for different wavelengths, when propagating through dispersive elements like prisms or gratings. Depending on the chosen method different things have to be kept in mind [54, 28].
When using optical fibers as a stretcher huge amounts of dispersion can be added. At the same time the fiber takes up very little space. At wavelengths of 1.5 µm there exist optical fibers which can add positive or negative dispersion to a pulse. However, at 1 µm, most of the transparent glasses and crystalline materials exhibit positive dispersion [11].
Propagating light pulses with high peak powers through optical fibers yields another consideration. With the propagation of the high-power pulses a nonlinear phase shift is getting accumulated. This means, that the light pulse is getting distorted by nonlinear effects like self-focussing or self-

phase modulation (SPM). A quantitative and dimensionless measure for this is the B-integral[42]

$$B = \frac{2\pi}{\lambda} \int_0^L n_2 I(z) \mathrm{d}z$$

where n_2 is the nonlinear refractive index, which depends on the intensity $I(z)$. This means, that pulses with high intensity accumulated higher nonlinear phase shift and therefore a higher B-integral. In principle, this phase shift, and therefore the value of the B-integral, is aimed to be kept low. At values of the B-integral > 1 already first broadening effects due to SPM arise. If the values get > 3 self-focussing starts, which can possibly damage the optical element [56] [42]. The following sections will introduce general dispersion theory. Afterwards, methods for stretching and compressing laser pulses are described, based on the now presented considerations. In the end of the chapter the theory for light amplification will be described.

2.2.1 Dispersion Theory

When talking about (chromatic) dispersion, the general understanding is, that the light is split up to different wavelengths when propagating through a transparent medium. This is due to the dependence of the refractive index of the medium on the wavelength (or frequency) of the incoming light $n(\lambda)$ ($n(\nu)$. Another way of describing this is the dependence of the phase and group velocity on the frequency of the light. Although a linear effect, dispersion has a huge impact on optical pulses. This can be evaluated by multiplying the electric field with an transfer function $H(\nu)$ [50]

$$V(\nu_{\mathsf{out}}) = H(\nu) V(\nu_{\mathsf{in}})$$

The transfer function $H(\nu)$ is a solution of the Helmholtz equation and is given by a frequency dependant wave number and the length of the dispersive medium. With a transfer function a shift of the spectral phase of laser pulses, propagating through a dispersive medium, can be described [11, 50].
The phase shift is subsequently evaluated by an inverse Fourier transformation of the electric field back to the time domain. For ultra-short pulses the spectral width is much smaller than the carrier frequency. To effectively evaluate the change in spectral phase $\Delta\phi$ when the optical pulse propagates through dispersive media one performs a Taylor series expansion around the carrier frequency [37]:

$$\phi(\omega) = \phi_0 + \frac{\Delta\phi(\omega)}{\Delta\omega}(\omega - \omega_0) + \frac{1}{2}\frac{\Delta^2\phi(\omega)}{\Delta\omega^2}(\omega - \omega_0)^2 + \frac{1}{6}\frac{\Delta^3\phi(\omega)}{\Delta\omega^3}(\omega - \omega_0)^3 + ... \quad (2.12)$$

Where the ω denotes the angular frequency and ω_0 the center frequency.
The zero-order term ϕ_0 describes a phase shift acting.
The first order term, or first order dispersion, is the group delay T_{G}, which is given by the group velocity v_{g}. It describes a delay of the pulse in time[52, 11]:

$$T_{\mathsf{G}} = \frac{1}{v_{\mathrm{g}}} = \beta' = \frac{d\beta}{d\omega}$$

The group velocity v_{g} changes with the central frequency ω_0. β is a propagation constant which depends on the frequency dependant refractive index $n(\omega)$ (also $n(\nu)$. Accordingly:

$$\tau_{\mathsf{d}} = \frac{z}{v_{\mathrm{g}}}$$

gives a time delay, also called group delay. Here z denotes the optical path length. In the same way, dispersion acts on the phase velocity v_p. Phase velocity means the propagation velocity of the wave front in the medium. By considering the phase velocity as[52]:

$$\frac{1}{c} = \frac{\beta(\omega_0)}{\omega_0} = \frac{n(\omega)}{c_0} = \frac{1}{v_\mathrm{p}}$$

where $n(\omega)$ is the frequency dependent refractive index. The influence of first order dispersion on the phase velocity shows, that it is by a factor $n(\omega)$ smaller than the group velocity. Note that, if the refractive index does not depend on the frequency and therefore $v = c$, as in an ideal nondispersive medium, the phase and group velocity are identical. [37] [52]

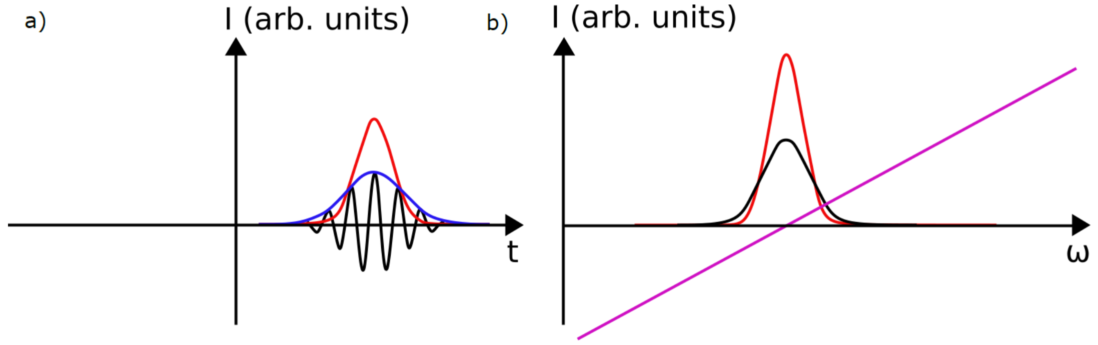

Figure 2.5: a) shows the time delay introduced by first order dispersion. b) shows the frequency domain with the linear phase in magenta. Adapted, with permission, from Jakob Fellinger [11].

The second order term of 2.12, also called group velocity dispersion (GVD), defines the difference in velocity for different wavelengths. This means different frequencies undergo different time delays and therefore the pulse spreads in time.

$$GVD = \frac{\mathrm{d}}{\mathrm{d}\omega}\frac{1}{v_\mathrm{g}} = \beta''$$

Generally, when the group velocity decreases with increasing optical frequency one speaks of normal dispersion. When the group velocity increases with decreasing wavelength one speaks of anomalous dispersion. [37, 52, 11]
A more concrete quantity for displaying dispersion is the dispersion coefficient:

$$D_\nu = \frac{\mathrm{d}}{\mathrm{d}\nu}\frac{1}{\nu} = 2\pi\beta'' \tag{2.13}$$

giving the temporal elongation of a pulse per unit length and spectral width. It can also be described in terms of wavelength as D_λ. If $D_\nu > 0$ (similarly $0 > D_\lambda$) normal dispersion is observed whereas $D_\nu < 0$ (similarly$0 < D_\lambda$ anomalous dispersion is observed [52]. Considering the group delay and deriving a second time one gets the group delay dispersion (GDD) as a quantitative measure of chromatic dispersion:

$$GDD = \frac{d}{d\omega}\tau_d = z\beta''$$

The GDD has the unit s^2/m whereas the GVD has the unit s^2, therefore, the GDD is the GVD per unit length.

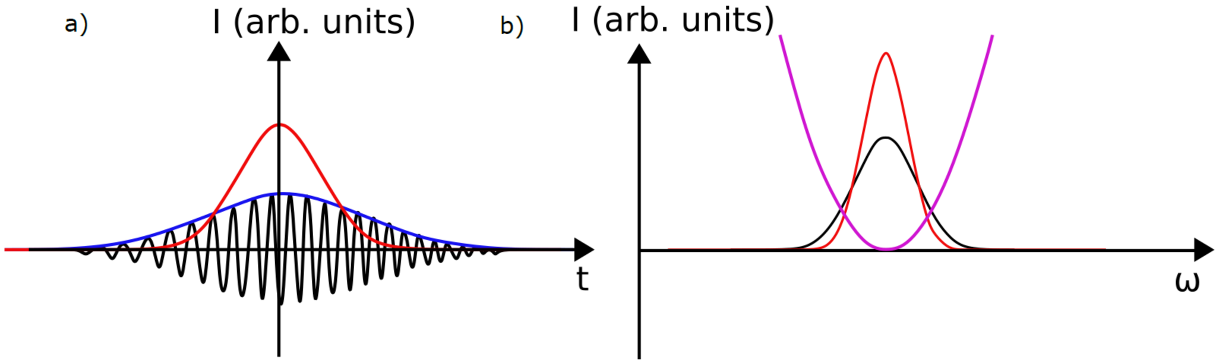

Figure 2.6: a) shows the second order dispersion in frequency domain in form of a broadening. b) shows the second order dispersion in frequency domain with the quadratic phase. Adapted, with permission, from Jakob Fellinger [11].

The last term, taken into consideration here is the third order dispersion (TOD). It is resulting from a dependence of the GDD on the optical frequency. The TOD also contributes to the elongation of pulses. However, it is not considered in the later work and therefore only mentioned here. [52]

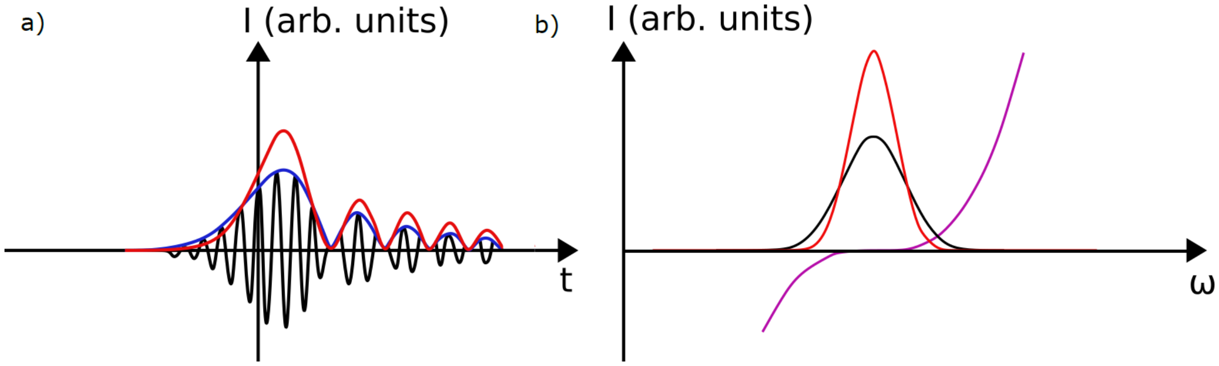

Figure 2.7: a) shows TOD in time domain. b) shows the TOD in frequency domain. Adapted, with permission, from Jakob Fellinger [11].

2.2.2 Dispersion Management

Propagation of Light Pulses in Dispersive Media

For simplicity, Gaussian pulses are considered to describe the propagation of light through dispersive media [50]:

$$A(t) = A_0 \text{exp}(\frac{-t^2}{\tau^2}) \text{exp}(\frac{j\alpha t^2}{\tau^2}) \tag{2.14}$$

Where $|A_0|\text{exp}(-t^2/\tau^2)$ is the complex envelope of the Gaussian, $\phi = \alpha t^2/\tau^2$ is the quadratic phase yielding an instantaneous frequency as a linear equation of time according to $\nu_i = \nu + \alpha t/\pi\tau^2$. The parameter α is called the chirp parameter. The chirp, an optical pulse is carrying, is the variation of the instantaneous frequency in time. A pulse is called up-chirped or positively chirped when ν_i is positive and negatively or down chirped if nu_i is negative. This can be shown by considering the phase of the pulse as a quadratic function of time [50]:

$$\phi(t) = \frac{\alpha t^2}{\tau^2} \tag{2.15}$$

where α is again the chirp parameter. By deriving $\phi(t)$ one gets the chirp parameter α according to:

$$\phi(t)'' = \frac{2a}{\tau^2} \iff a = \frac{\phi(t)''\tau^2}{2} \tag{2.16}$$

By performing a Fourier transformation on the optical pulse one gets a representation in the frequency domain:

$$A(\nu) = \frac{A_0\tau}{2\sqrt{\pi(1-ja)}}\text{exp}[-\frac{\pi^2\tau^2\nu^2}{1-ja}] \tag{2.17}$$

$$S(\nu) = \frac{I_0\tau^2}{4\pi\sqrt{1+a^2}}\text{exp}[-\frac{2\pi^2\tau^2(\nu-\nu_0)^2}{1+a^2} \tag{2.18}$$

where $\psi(\nu) = -2\pi^2\tau^2[a/(1+a^2)]\nu^2$ is the spectral phase. $A(\nu)$ is the envelope function and $S(\nu)$ the spectral intensity[50].
When a Gaussian pulse is propagating through dispersive media, it can again e described by a transfer function acting on it. This transfer function introduces a quadratic phase term depending on time, $\psi(f) = b\pi^2 f^2$, to the electric field of the light pulse. The resulting transfer function is:

$$\text{H}_e(f) = \text{exp}(-jb\pi^2 f^2)$$

With b being the chirp coefficient introduced to the pulse by the dispersive medium. Performing an inverse Fourier transformation yields the corresponding response function as a Gaussian function in time:

$$\text{h}_e(t) = \frac{1}{\sqrt{h\pi b}}\text{exp}(jt^2/b) \tag{2.19}$$

A Gaussian pulse with a constant phase, which has a minimum product of spectral and temporal width, is called bandwidth limited (or transform limited). The pulse duration of a Gaussian pulse is the full width at half maximum (FWHM) value from the time dependent intensity $I(t)$:

$$\tau_P = \sqrt{\frac{2\text{ln}(2)}{\Gamma_1}}$$

where the bandwidth of the pulse is the FWHM in frequency domain of the electric field:

$$\delta\nu = \frac{\delta\omega}{1\pi}\sqrt{\Gamma_1(1+\frac{\Gamma_2}{\Gamma_1})^2}$$

putting those two values in relation one gets the time bandwidth product, the condition for a Gaussian pulse to be transform limited:

$$\tau_P\delta\nu = \frac{2\text{ln}2}{\pi}\sqrt{1+(\frac{\Gamma_2}{\Gamma_1})^2} = 0.44\sqrt{1+(\frac{\Gamma_2}{\Gamma_1})^2}$$

here the parameters Γ denotes the chirp of the pulse. This means, if a pulse gains chirp it spreads in the time domain. In other words when a bandwidth limited pulse propagates through a dispersive medium it is elongated in time.[50]
For a chirped Gaussian pulse, a similar thing happens and it is altered as it propagates through a dispersive medium. Depending on the sign of the initial chirp of the pulse and the sign of the chirp added through the dispersive medium it is either elongated or compressed in time. It has to be kept in mind, that, by propagation through a dispersive medium, only the temporal width of the pulse changes. The dispersive medium has no effect on the spectral width of the pulse [50].

Stretching

When speaking of stretching a light pulse means to broaden it in time. There are several ways to introduce dispersion such that a pulse is stretched. This can be done, as already discussed, by propagating the light pulse through dispersive media like fibers, prisms or gratings [50]. However, one has to consider which way is the most convenient.
The propagation of a light pulse through a fiber for instance, can be approximated by a transfer function. Similar to the priorly discussed case, chirp is added to the pulse [50]:

$$h_e(\nu) = \text{exp}[-j\Psi(f)]$$

During propagation, different spectral components propagate through the fiber with different group velocities. Therefore, they are getting delayed in time relatively to each other, thus, chirp is added to the pulse:

$$b = 2\beta'' z = \frac{D_\nu}{\pi} z$$

Here z denotes the propagation direction. D_ν is the chirp parameter from equation 2.13, which means that through the fiber GVD is added to the pulse. If $D_\nu > 0$ positive GVD is added and the propagation through the fiber acts up-chirping on the pulse. For $D_\nu < 0$ the propagation is down-chirping. Note that, when the pulse is entering the fiber negatively chirped, and positive GVD is added, it is first compressed until its transform limit and afterwards stretched (up-chirped) [50].

As described by the B-integral, propagating a pulse through a fiber can lead to severe (or damaging) nonlinear effects [56]. To evade this problems, one can use a combination of gratings or prisms. Historically, it was only possible to introduce negative GVD with the use of gratings and prisms. Thus, *Martinez et al.* introduced a design, where a lens telescope is added between two gratings to introduce positive GVD to an optical pulse [27] [28]. The design is displayed in figure 2.8. This configuration yields two main benefits. First, depending on the position of the telescope, the sign of dispersion can be flipped from negative to positive dispersion . Second, the telescope introduces angular magnification. This leads to an increase of the GVD acting on the pulse through the gratings. Thus, high amounts of GVD can be introduced by this design. However, with the rise of the added GVD, the distance between the gratings rises and the setup needs more space. The general dispersion introduced by the stretcher/compressor design is [27]:

$$\frac{d^2\phi}{d\omega^2} = k\beta'^2 z_3 = k\beta^2(z_1 + M^2 z_2) \tag{2.20}$$

In the figure 2.8 z_i denotes the position of the gratings with respect to the focal planes F_i of the lenses. If the the gratings are placed before the focal plane F_i, z_i is positive and it is negative if the grating is placed between the lens and the focal plane. Combining that knowledge with equation 2.20 a flip of the sign of added dispersion can be obtained if either one of the gratings is put such that a negative value is obtained[27]. The factor $M = f_1/f_2$ is the angular magnification of the telescope. When it is compared with the dispersion added, it enhances the dispersion by a factor of M^2. Note, that for a double pass scheme an additional factor of 2 is introduced and furthermore, problems with astigmatism and lateral walk-off are evaded. With this configuration it was shown, that dispersion comparable to fibers with a length of up to 100 km can be compensated [27] [28].

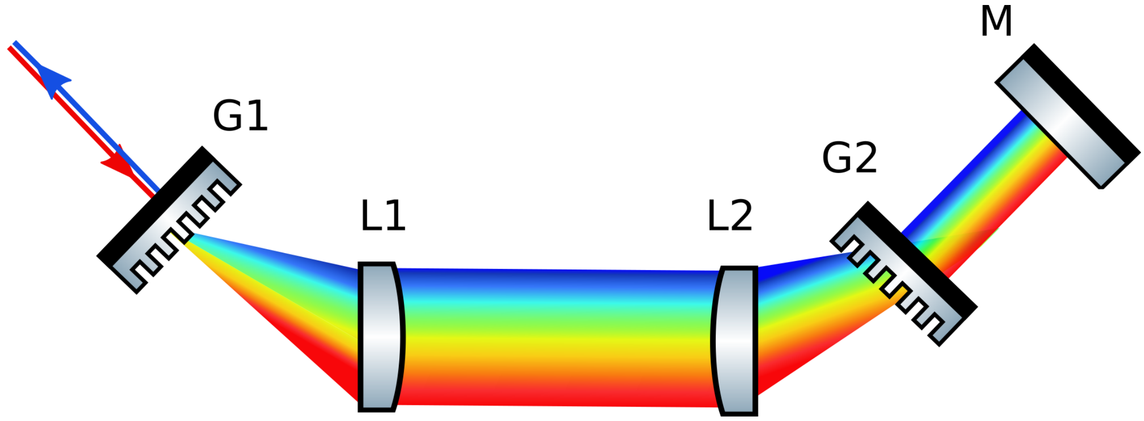

Figure 2.8: shows a Martinez type stretching scheme. The beam is spatially dispersed at grating G1. Lens L1 collimates the beam and lens L2 focusses the beam behind grating G2. With the focal point being behind G2 the chirp of the light pulse is inverted as described i the section 2.2.2. With the red part of the spectrum taking a longer optical path than the blue part, stretching takes place.

Compression

After the amplification (section 2.2.3) in the CPA, the pulses have to be compressed. A very common way to compress pulses is with the help of optical elements which introduce an angular dispersion, such as gratings and prisms. The pulse is spread in space (dispersed) into different frequencies by the first dispersive element. The optical path length of different frequencies differs, such that a phase shift is encountered [50]

$$\Psi(\nu) = \frac{2\pi\nu}{c} l_0 \cos(\theta(\nu))$$

yielding a transfer function:

$$h(\nu) = \exp(-j\Psi(\nu))$$

A second dispersive element, for instance a second grating, removes the angular chirp, such that the different spectral components propagate parallel to each other. Two further gratings reverse the process again, such that the light is focussed by the third grating to the fourth grating which collimates the beam/pulses again. Instead of the two additional gratings a retro-reflector mirror, shifting the outgoing beam spatially parallel to incoming beam, can be used. The angular dispersion chirp coefficient of a so-called double pass grating compressor is:

$$b \; - \frac{l_0}{\pi\lambda_0}\alpha_\nu^2$$

where α_ν is the angular dispersion coefficient. This yields a parameter b, which is always negative. In case of diffraction gratings e.g. grating compressor the GDD is given by [54]:

$$GDD_{\text{grating}}(\lambda) = -\frac{\lambda^3 d}{\pi^2 \Lambda_g^2}(1 - (\frac{\lambda}{\Lambda_g} - \sin(\alpha)^2)^{\frac{2}{3}} \qquad (2.21)$$

Here, d is the distance between the two gratings, Λ is the groove density of the gratings and α is the incident angle, with which the pulse train hits the first grating.

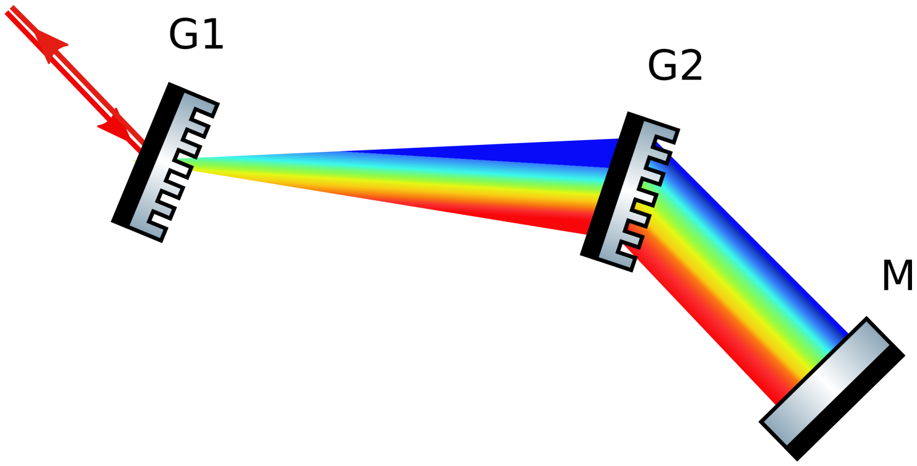

Figure 2.9: A compression scheme of a Treacy type compressor is shown. Grating G1 disperses the beam spatially and grating G2 brings the spectral components back to be parallel to each other. Afterwards the light is folded back by a retro-reflector mirror M and the processes is repeated/inverted. As can be seen, the blue part of the light takes a longer path leading to compression.

2.2.3 Light Amplification

Interactions Between Atoms and Photons

Laser amplification is based on the interaction of light with atoms. The Boltzmann distribution describes the distribution of the energy states of the atoms. Based on that, the basic interactions can be described [51].

$$P(E_m) \propto \text{exp}(\frac{-E_m}{k_\text{b}T}) \tag{2.22}$$

Here, P(E_m) is the probability an energy level is occupied, E_m is an arbitrary energy level, k_B is the Boltzmann constant and T is the temperature.
There are three fundamental interactions of photons and atoms in laser generation. When an atom has an energy state E_2 which lies on a higher energy level than an energy level E_1, it can spontaneously decay into an Energy state E_1 and emit a photon $h\nu$ with a distinct energy and therefore wavelength. This process is called spontaneous emission. Its probability density depends on the frequency ν of the transition [49]:

$$p_\text{sp} = \frac{c}{V}\sigma(\nu)$$

where $\sigma(\nu)$ is the transition cross section and V denotes the volume of the cavity.
Two possible interactions arise in the case of an photon encountering an atom. If the atom is initially in the lower energy E_1 level, the photon can be absorbed/annihilated by the atom. If the atom is occupying the upper energy level E_2 it may be stimulated to go to the lower energy level by emitting the excess energy via a photon with the exact energy/frequency hν of the atomic transition. The two effects are called absorption and stimulated emission, respectively. Since they describe the same transition, but in opposite direction the probability density p_st and p_ab is the same [19]:

$$p_\text{st} = p_\text{ab} = \frac{c}{V}\sigma(\nu)$$

The third of the priorly discussed interactions is responsible for laser amplification, whereas absorption on the other hand is responsible for attenuation and spontaneous emission, which is accountable for the amplifier noise, based on ASE [51]. The probability density for both, absorption and stimulated emission can be written as

$$W_{\text{i}} = \phi\sigma(\nu) \tag{2.23}$$

where

$$\sigma(\nu) = (\frac{\lambda^2}{8\pi t_{\text{sp}}})g(\nu) \tag{2.24}$$

Is the transition cross-section at a frequency ν, t_{sp} is the lifetime and $g(\nu)$ is the lineshape function, modelling the spectral lineshape of the emission [49]. The density of the absorbed photons and the photons leading to stimulated emission can be written as $N_{\text{i}}W_{\text{i}}$, leading to the net number of gained photons per second and unit volume as NW_{i} with $N = N_2 - N_1$. N specifies the difference in population density. If it is positive population inversion is at hand and the (gain-)medium can act as amplifier. To obtain population inversion energy has to be applied to the system, by an external pump. In case of an optical fiber, the gain medium has the form of an cylinder of the volume dz. When the lasing process starts, the gain volume exhibits a photon flux $d\phi(z)$. The mean number of photons in the gain material can therefore be described as [51]:

$$\text{d}\phi = NW_{\text{i}}\text{d}z \tag{2.25}$$

Knowing the probability density for stimulated emission (equation 2.23), equation 2.25 can be rewritten in form of a differential equation [51]

$$\frac{\text{d}\phi(z)}{\text{d}z} = \gamma(\nu)\phi(z) \tag{2.26}$$

Where $\gamma(\nu)$ is the gain coefficient, which gives the gain obtained in the gain medium:

$$\gamma(\nu) = N\sigma(\nu) = N\frac{\lambda^2}{8\pi t_{\text{sp}}}g(\nu) \tag{2.27}$$

By solving 2.26, the gain dependant optical intensity is given by:

$$I(z) = I(0)\text{exp}[\gamma(\nu)z] \tag{2.28}$$

Note, that in the case of attenuation the exponential of I(z) gets a negative sign, showing a decrease of the intensity when propagating through a gain medium.
In a gain medium like a fiber with length d, the total gain is given by the ratio of the input and output photons.[19] [51]:

$$G(\nu) = \text{exp}[\gamma(\nu)d] \tag{2.29}$$

Laser Gain and Saturation

When the input power reaches a certain level the pump power of the amplifier medium and with that the population inversion decreases which leads to a decrease in gain also called gain saturation. There are several different effects happening depending on the type of gain medium and type of input signal. In a steady state, for instance, where long time scales are considered and therefore the resonator losses and pump power are constant, the gain can be written as [19]:

$$G = \frac{g_{\text{ss}}}{1 + \frac{\tau_g P}{E_{\text{sat}}}} = \frac{g_{ss}}{1 + \frac{P}{P_{\text{sat}}}} \tag{2.30}$$

Here g_{ss} is the small signal gain, which is the obtained gain if no saturation is at hand. However, if the signal power equals the saturation power P_{sat} the gain is reduced to half the small signal gain [19].
In the case of the input signal being an short optical pulse, such that spontaneous emission is negligible, the gain after the pulse train is amplified, thus stimulated emission is happening, is reduced by a factor exp($\frac{-E_p}{E_{\text{sat}}}$) [19].
E_{sat} is the saturation energy. The effective gain which is experienced by a pulse can be determined by the Frantz-Nodvik equation. In the case of strong saturation effects for optical pulses in, for instance, fiber amplifiers the pulse shape can be significantly distorted. Moreover, in the case of inhomogeneous saturation, also the spectral shape of the pulse is modified. However, many fiber amplifier systems are often operated in a strong saturation regime to achieve the highest average output power and conversion efficiency. If the gain medium is saturate by the input signal ASE is minimized, the population inversion is high, and most of the atoms interact by stimulated emission. Therefore, the conversion from pump energy to signal energy is the highest [34, 35].

Chapter 3

Seed Laser

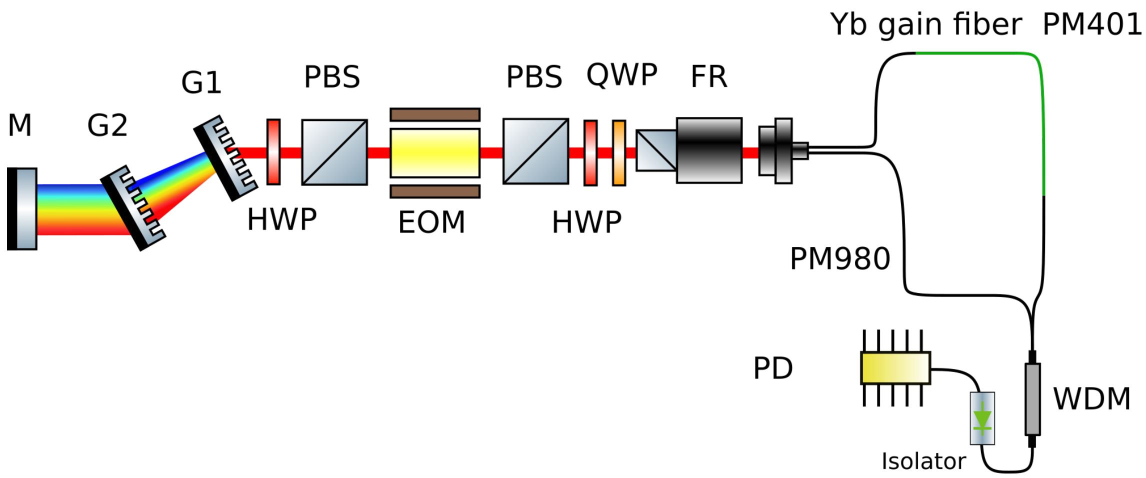

Figure 3.1: Schematic view of the figure-9 design as used in the setup. PD is the pump diode, afterwards follows a fiber-coupled isolator preventing back reflections. Before the loop is a wavelength division multiplexer (WDM) which provides, that the light stays in the fiber loop. The fiber loop consists of a polarization maintaining (PM 980) fiber and an asymmetrically placed polarization maintaining Yb-gain fiber (CorActive-Yb-401-PM). The free-space section consists of an Faraday rotator (FR), a combination of quarter and half wave plates (QWP, HWP). The light will be coupled out of the cavity by polarizing beam splitter (PBS). For the stabilization an EOM is place. The dispersion management is realized by a combination of gratings (G1, G2). The end mirror (M) closes the cavity.

The foundation of a laser system is the seed laser. The seed laser is providing the light, which will get amplified in later stages. Therefore, and depending on the application, the design for the seed laser is crucial. For precision spectroscopy a robust design, which is stable to environmental influences, is needed. Moreover, easy handling with a reproducible ML state, providing the stabilization of the repetition rate and CEO is crucial. To receive precise spectroscopic measurements, the laser system itself must be designed to be in a low noise regime, RIN and PN respectively. For amplifying the laser signal, the pulses resulting from the oscillator need to have sufficient energy to saturate the fiber amplifier. Therefore, the low noise properties can be kept and sufficient gain results from the individual amplification stages (See section 3.3). The seed laser for this setup is therefore based on all fiber geometry. For a detailed description of fiber lasers, their properties and advantages can be read in [4] and [18]. The used seed laser geometry in this work is based on the work of *Mayer et al.* [31]. However, a recap of the most important ML techniques in fiber-based seed lasers is provided. Thus, supporting the design criteria, used for the seed source in the system at hand.

A design based on nonlinear polarization evolution (NPE) in combination with non-polarization maintaining fibers, for instance, allows for an easy design with widely available off-the-shelf components. However, it suffers from drawbacks due to the non-polarization maintaining (PM) fibers lack of robustness over mechanical stress or it's sensitivity over humidity and temperature fluctuations [29]. By implementing PM fibers in the design the disadvantages due to environmental effects got disposed and successful ML via cross splicing has been shown [57].
The nonlinear amplifying loop mirror NALM and nonlinear optical loop mirrors (NOLM) [8, 13] represent further possibilities for designing ML lasers in a PM fiber design. Both designs are based on the propagation of two electromagnetic waves, clockwise and counterclockwise, through a fiber loop introducing a nonlinear phase shift between each other. The reflection and transmission of the fiber loop mirror depends on the difference in the nonlinear phase shift, which itself is intensity dependant, allowing for ML in the loop mirror. In the case of the NOLM, placing a beamsplitter with unequal splitting ratio, is enough to introduce the nonlinear phase shift bigger than zero [31].
In the case of the NALM design, a gain fiber is placed asymmetrically into the loop, causing different amplification and nonlinearities to each wave [11, 31]. Therefore a difference in the nonlinear phase shift is obtained. Due to the amplification combined with the different path lengths, the two light-waves sustain unequal phase delays.
By attaching the fiber ends of the output port of the NOLM or NALM to each other, the laser is put in the "figure-8" configuration [9]. This configuration allows for ML, but to get it to a self-starting ML state is not a trivial task [32]. A non-reciprocal phase bias has to be introduced to the design, by placing waveplates and a Faraday rotator in the form of a free-space section [22, 17]. Nonetheless, the figure-8 design experiences drawbacks, since is not possible to operate it at high repetition rates. This is mainly due to the fact, that the length of the two different fiber-loops cannot be changed arbitrarily [11]. Furthermore, the figure-8 laser is in a closed loop design, resulting in not having a cavity end mirror. Hence, a piezoelectric actuator, required for stabilizing the laser cavity, cannot be mounted [31].
Further improvement has been introduced with the figure-9 configuration. Here, one of the loops of the figure-8 configuration is straitened to a freespace section. In the end of the freespace section a mirror is placed coupling the light back into the fiber loop [20]. This design makes a versatile handling of the laser possible and stabilization of the repetition rate via an mirror mounted on a piezoelectric actuator can be achieved [20]. The figure-9 laser can be operated based on many different gain materials like Yb, Er and Tm/Ho [16]. It has been shown that repetition rates up to 700 MHz, can be generated [23]. Furthermore, the figure 9 configuration in an all PM design allows for high power scalability by the help of LMA fibers, allowing for average powers up to 2 W at 72 MHz of repetition rate [24].
By putting a grating pair in the free-space section of the cavity, the laser dispersion and therefore output pulses can be arbitrarily tuned to different ML states [16]. Recently *Mayer et al.* have characterized versatile laser design options, yielding different ML states of the figure 9. A ML state can be obtained resulting in low noise quantities, by tuning a grating compressor inside the laser cavity [31].

3.1 Setup Description

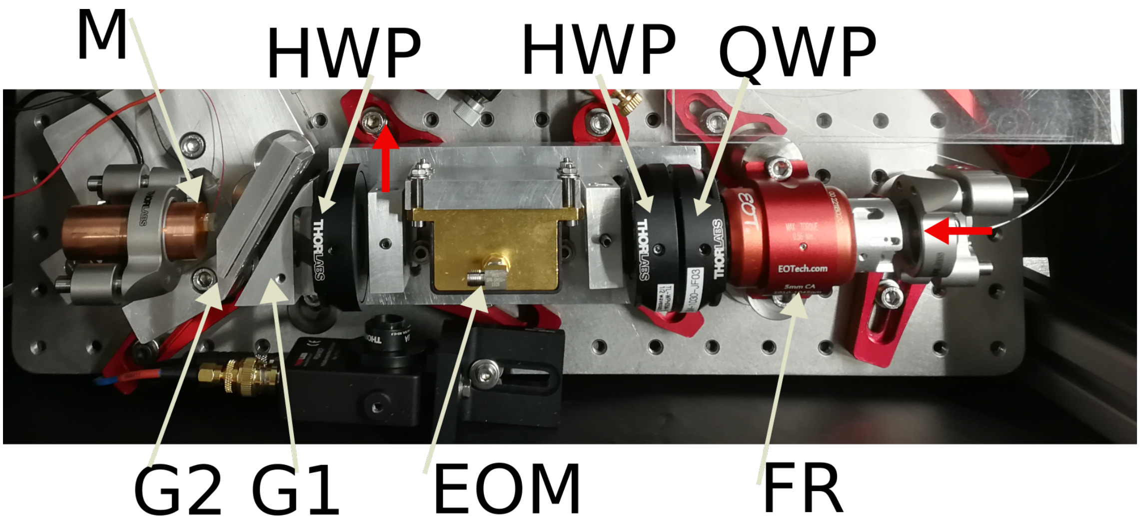

Figure 3.2: The free-space section of the seed laser cavity as described in detail by the scheme 3.1 is shown. Two red arrows mark the light path. M is the end-mirror, G2 and G1 form the grating compressor. HWP denote the λ/2 waveplates and QWP denotes the λ/4 waveplates. FR is the Faraday rotator.

The seed laser, used in the system, is based on a figure-9 configuration. It is based on a all PM NALM with non-reciprocal phase bias as described by *Mayer et al.* The design was chosen for its reliable self-starting behaviour with reproducible ML parameters, like the spectra, intra cavity dispersion, chirp, and output power. Moreover, the cavity end mirror gives the possibility for active stabilization, required for making the OFC applicable in precision spectroscopy. Particular focus was put on the properties of the low RIN and PN. Therefore, the laser operates in a slightly negative near zero intra cavity dispersion regime.
The oscillator consists of a fiber section consisting of polarization maintaining fiber (PM 980) and 42.5 cm long Yb-gain fiber (CorActive-Yb-401-PM). A 300 mW power Fiber-Bragg-Grating (FBG) stabilized diode is connected to the fiber loop via an WDM. The free-space section consists of a Faraday rotator, 2 $\lambda/2$ waveplates and one $\lambda/4$ waveplate, an EOM and a grating compressor. A detailed scheme can be seen in 3.1, a picture of the oscillator is seen in figure 3.2.
With the polarization optics (waveplates, Faraday rotator) in combination with the asymmetrically placed and pumped gain fiber, a nonlinear phase shift is introduced. Furthermore, the NPR design allows for a self-starting ML state. The grating compressor provides dispersion tuning to generate different operation regimes. The EOM inside the cavity as well as the end mirror, which is placed on a piezo actuator into a heavy bullet mount, allows to apply a stabilization scheme. The seed laser is mounted on a separate breadboard, which is additionally damped by sorbothane isolator. With this mechanical and acoustic noise introduced the environment of the laser are avoided. The chosen design and operation regime yields pulses with a repetition rate of $f_{\text{rep}} = 132.4$ MHz.

3.2 Results

The pulses were characterised using the method of second harmonic generation (SHG) frequency resolved optical gating (FROG), based on a Type 1 phase matching 50 µm thick BBO crystal. The laser is operating in a close to zero, slightly negative dispersion regime. Thus, the pulses are getting stretched and compressed at different positions in the cavity. With the output-port

of the laser near the diffraction grating pair, the pulses are negatively chirped and have a pulse duration of 1 ps.
The obtained spectrum has a bandwidth of about 60 nm, with a peak at about 1070 nm. The average output power is 35 mW ($E = 220$ pJ).

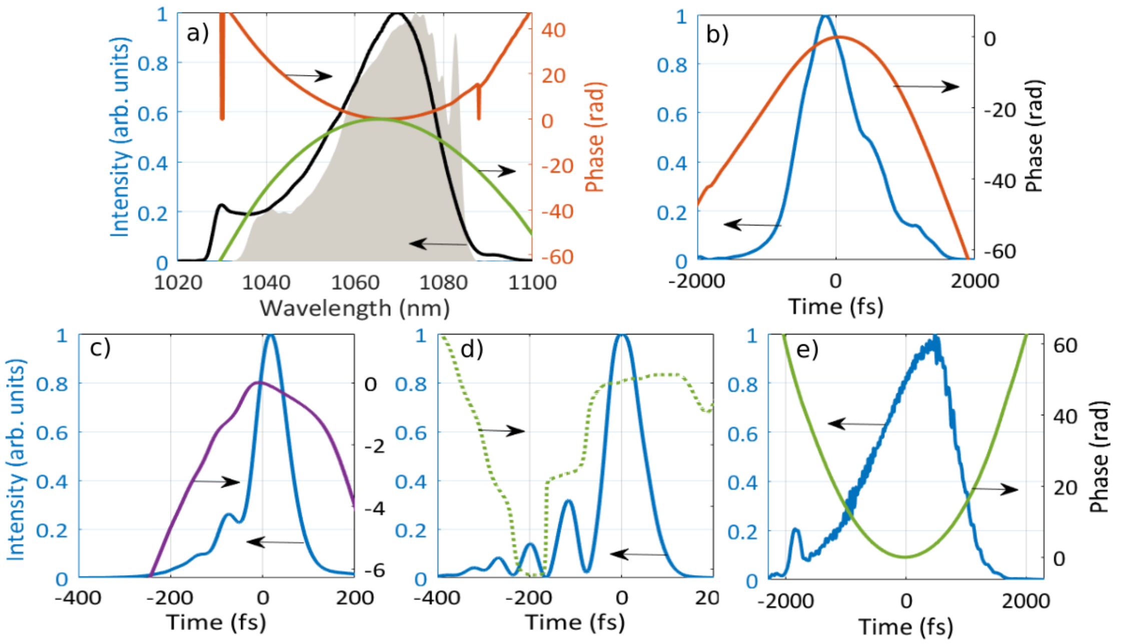

Figure 3.3: a) shows the spectrum measured with the Ando spectrometer (AQ6315A Ando Yokogawa optical spectrum analyser (OSA)) in black and in grey the retrieved spectrum from the SHG-FROG apparatus. b) shows the temporal envelope after propagating 1.5 mW pulses through free-space optics, c) after propagating the same 1.5 mW pulses through 1 m of fiber. d) shows 35 mW pulses after propagating through 1 m of fiber. e) gives the temporal shape of the pulse after the stretcher. Reprinted with permission of Valentina Shumakova [44].

The pulses from the oscillator were propagated through different lengths of fiber. This was made, on the one hand, to evaluate on effects of dispersion and nonlinearities introduced from fibers and evaluate possible options guiding the pulse train to the stretcher section for the CPA. On the other hand, feasible stretching schemes have to be evaluated. Moreover, by propagating the beam through dispersive media, the sign of the chirp can be estimated.
Figure 3.3 shows pulses of different average powers after propagating through 1 m of fiber. A comparison is made with the pulse propagating via free-space optics (b)). The initial pulses had an average power of 1.5 mW. The propagation of those light pulses through 1 m of fiber is seen in panel c). It can be seen that the pulses, compared to those propagating in free-space, are getting compressed. Thus, the negative chirp of the initial pulses is verified. Furthermore, appearance of SPM can be seen.
Panel d) shows the same initial pulses with more energy ($\sim$ 35 mW) propagating through 1 m of fiber. More power can be applied by tuning the $\lambda/2$ waveplate before the grating compressor (3.2. With more average power the effects of SPM and self-steepening are getting more severe. Panel a) of the figure shows the measured spectrum with the spectrometer (AQ6315A Ando Yokogawa OSA) in black. The grey shaded area is the retrieved spectrum from the SHG-FROG apparatus. To not introduce broadening of the pulses by SPM, a short fiber was used to guide the pulses from the oscillator breadboard to the stretcher. Moreover, the combination of free-space stretcher to change the sign of the chirp and afterwards propagating it through a fiber stretcher was chosen.

Chapter 4

Chirped Pulse Amplifier

4.1 CPA Design

The core of this thesis deals with the development and characterization of an high average power laser amplifier. High average power Yb:fiber amplifier systems are gaining more and more attention, since they are reliable laser systems, which are simple to build with off the shelf components [21] [4]. Their scaleability to high peak and average powers is rising the interest in a wide range of applications, starting from material processing [2], going over to laser wakefield particle acceleration [1], remote sensing and ranging [12], and in the presented case high precision spectroscopy.
Fibers have shown to be a good option for amplifying light, because of their large surface to volume ratio, easing thermal management [31]. Moreover, fiber-systems have gained much attention, because of their scalability, simplicity, and easy development with off the shelf components. A general concern in using fiber systems, especially for high average powers, is damaging active and passive optical elements. The use of LMAs and PCFs, active and passive fibers paved the way for generating high average powers, based on common methods like SSA and CPA [21, 25, 26] Using SSA for amplifying to high average powers yields pulse durations in the range of 60-90 fs with a bandwidth containing several tens of nm, while obtaining average powers of 100 W [60]. Nevertheless, this method works mainly in a nonlinear regime. This rises the problem of degrading the comb properties by, for instance, coupling RIN to PN, via processes like SPM or self-steepening. Thus, the method is unsuitable for precision spectroscopy.
In contrast to SSA, CPA works in a linear regime, minimizing the accumulation of nonlinear phase. It was originally introduced in 1985 by Donna Strickland and Gerard Mourou for the use in telecommunication fiber lasers [47]. However, with the technical advances in fiber processing, the method had huge impact on physics, enabling pulse trains with average powers in the kW region [43], ultimately gaining them the Nobel prize for physics in 2018. As described before, the principle is based on stretching the pulses prior to amplification and finally compressing them again, thus minimizing temporal intensity in the gain material, hence suppressing rising nonlinearities and reducing the risk of damaging active and passive optical elements. Various design options for stretching and compressing optical pulses have been presented, including the arrangement of a pair of diffraction gratings, namely the Treacy and Martinez configuration, which are the main methods used in the presented work [54, 28].

4.2 CPA Setup Description

4.2.1 Stretcher and Spectral Tunability

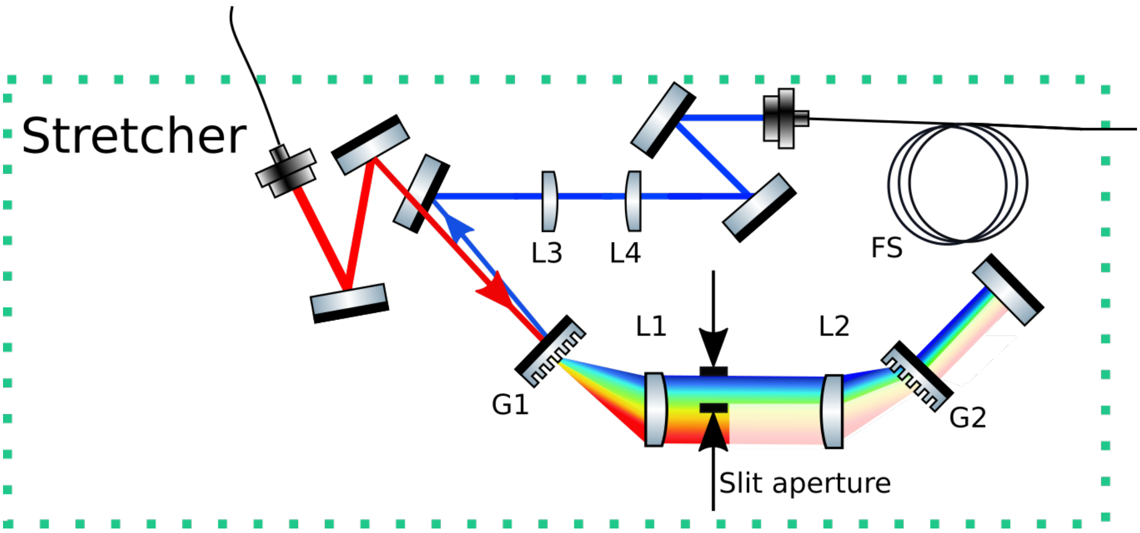

Figure 4.1: The full setup of the stretcher, including the free-space and fiber section, is shown. Starting from the left side the beam gets coupled to free-space and then guided to the Martinez stretcher by two mirrors. The Martinez stretcher consists of two gratings G1 and G2, L1 and L2 form the lens telescope and M depicts the retro-reflector mirror. The slit-type aperture is denoted with SLIT and two arrows. After the slit, the cropped spectrum is indicated by a pale area. Afterwards the beam propagates through a lens telescope L3 and L4 and gets coupled to the fiber stretcher FS.

The laser pulses, generated in the seed oscillator are guided from the dispatched oscillator breadboard to the Martinez stretcher, by 20 cm fiber (Thorlabs PM-980), which assures to maintain the pointing stability of the beam. The length of this fiber was chosen to not introduce further disturbances due to nonlinearities as discussed in section 3.2.
The used gratings (G1 and G2 in 4.1) for the free-space stretcher are two transmission diffraction gratings with a grid spacing of 1600 mm^{-1} (LightSmith Technologies, T-1600-1030s). As discussed in section 2.2.2 a Martinez configuration is used to flip the sign of the chirp, yielding a huge stretching factor and avoiding possible rising nonlinearities. A telescope consisting of two cylindrical lenses of 50 mm focal length (Thorlabs LJ1695L2-B) is used to collimate and refocus the beam between the gratings. After the stretcher a retro reflector is placed (M), such that a double pass of the stretcher and thereby a higher GVD is obtained. By placing another cylindrical lens telescope (L3 and L4), with focal lengths 2.5 cm and 5 cm respectively, after the stretcher, astigmatism is compensated.
The incoming pulses before the stretcher have a pulse duration of 800 fs with negative chirp and an average power of 25 mW. After the stretcher they have positive chirp with a pulse duration of 1.5 ps. The average power after stretching is 15 mW. In the following, the pulse train is coupled to a 110 m fiber stretcher (4.1 FS) (Thorlabs PM-980), which further stretches the pulses to 110 ps of pulse duration and directly couples them to the following amplification stages.
Additionally, in the Martinez stretcher a slit type aperture has been placed (figure 4.1 SLIT). The aperture is place between the two lenses (L1 and L2) of the first telescope. This allows for an arbitrary spectral tuning while the beam is spatially dispersed and already has been collimated by the first lens. The tuning allows at the same time for a modification of the temporal shape of the pulse. A detailed evaluation of the spectral tuning can be seen in 4.3.

4.2.2 Amplification Chain and Grating Compressor

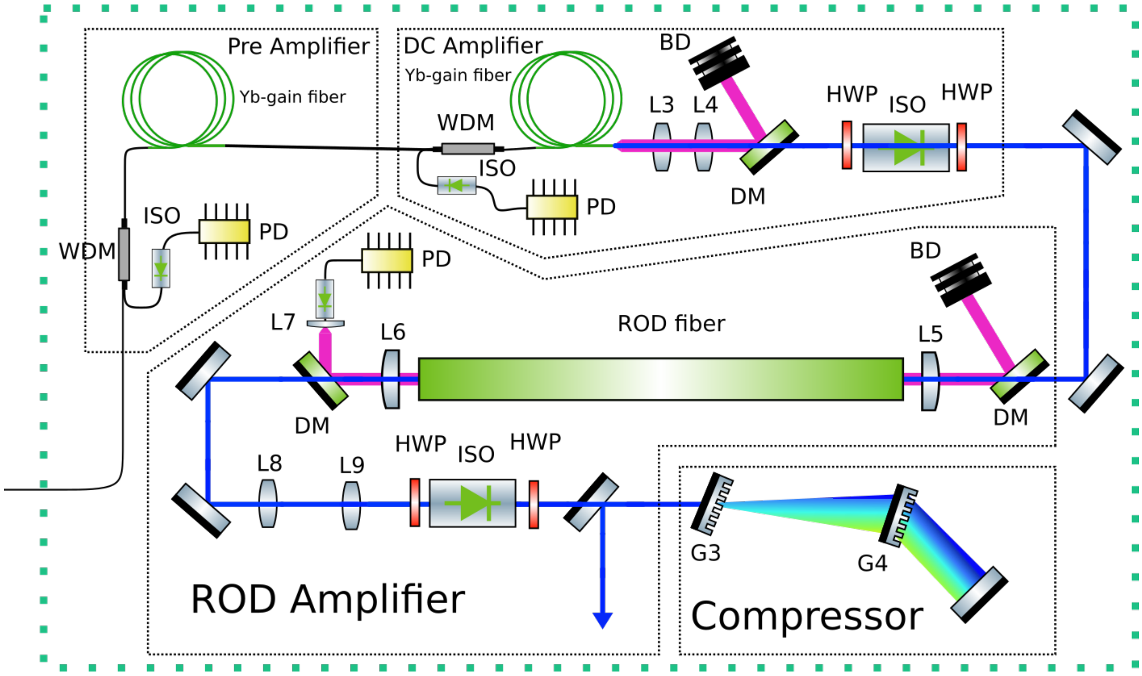

Figure 4.2: A scheme of the amplification chain and grating compressor is shown. Every amplification stage is surrounded by a dotted line. PD denotes the pump diode at each stage, which couples the pump light via an WDM to the gain fibers. L3 is the out-coupling lens of the light from the fiber of the second stage. DM denotes a dichroic mirror, filtering the unabsorbed pump light at every stage. HWP denotes half waveplates, which in combination with isolators (ISO) prevent light back-reflections. Fiber coupled isolators are also used at the pump diodes for the same reasons. L4 is the incoupling lens for the second high power amplification stage, which additionally couples out the pump light for this stage. The same way, L5 is the incoupling lens for the pump light of the second high power stage and outcoupling lens of the amplified light of that stage. L6 couples out the pump light from the second high power stage pump diode. L7 and L8 form a lens telescope. G3 and G4 form the grating compressor. The excessive pump light of both high power stages gets dumped on a beam dump (BD)

Following the stretcher, the light pulses are amplified by a three-stage amplifier chain. The first two stages are directly connected (spliced) to the fiber stretcher and implemented in an all-fiber design.
The pre amplification stage consists of an Yb-doped PM fiber (CorActive Inc., Yb 01-PM; 4.2 - Yb-gain fiber). The gain fiber is pumped by a FBG stabilized Laser diode (Thorlabs BL976-PAG700; 4.2 - PD) which has a center wavelength of 976 nm and controlled by a compact laser Diode controller (Thorlabs, CLD 101x). The pump diode is spliced to the gain fiber via an PM Filter and WDM (Advanced Fiber Resources, LTD., PM FWDM Series).
The first high power stage is build from a 2 m double clad (DC) fiber (LIEKKI/nLight Yb1200-10/125DC-PM) which is pumped by an Conduction cooled, 20 W fiber-coupled diode laser module (Coherent - DILAS Diodenlaser GmBh) and connected to the PM pump and signal combiner (Advanced Fiber Resources, PMMPC Series). To prevent the Fresnel back reflection from being amplified, the fiber output is angularly cleaved to 8°. After the fiber a lens (L3) is placed to collimate the beam to 2.3 mm diameter. Therefore the tip itself is put on a XYZ translation stage to have better control on the distance between the lens and the fiber output. To collimate the beam a lens (L4) with 25.4 mm focal length is placed after the stage. The lens is placed with a tilt, to compensate the angular cleavage of the fiber. A dichroic mirror (DM) is placed

to filter out the unabsorbed pump, such that it would not disturb following stages. Afterwards, a combination of half waveplates (HWP) and a Faraday isolator (ISO) to prevent an damaging amplification of back-reflections are placed.
A lens with a focal length of 60 mm (L5) couples the light to a water cooled large-pitch PCF (4.2 - ROD fiber) (NKT Photonics Inc, aeroGAIN-ROD module) with a length of 80 cm. The fiber is backwards pumped by a 240 W conduction cooled fiber coupled laser diode at 976 nm (DILAS - 976nm, Conduction-Cooled, Narrow Linewidth, Fiber- Coupled, Multi- Bar Module,) in the opposite direction of beam propagation to reduce nonlinear effects. Therefore another dichroic mirror (DM) is placed bevor the incoupling lens to filter out the residual pump light.
The pump is coupled to the ROD fiber by a lens (L6) with a focal length of 32 mm. After the ROD fiber a telescope consisting of two lenses (L8 and L9) with focal distances of -100 mm and 200 mm, to expand the beam and prevent damage of following optics is placed. The beam propagates through a half waveplate (HWP) isolator (ISO) combination to prevent amplification of back-reflections and damaging of the fiber.
The re-compression takes place in a Treacy type grating compressor. To withstand the high peak and average powers, bulk transmission gratings were used (LightSmyth Technologies, T-1600-1030s Series; 4.2 - G3 and G4). The gratings have a groove density of 1600 lines per millimetre.

4.3 Results

4.3.1 Spectral Tuning

As described in section 4.2.1, the slit type aperture in the stretcher allows for an arbitrary spectral tuning, while the beam is spatially dispersed. Different spectra at different slit position, resulting in a different spectral bandwidths as we narrow the opening of the slit, were measured. The different spectra are seen in c) of figure 4.3. The measurements were taken with an AQ6315A Ando Yokogawa optical spectrum analyser (OSA). With the measurements of SHG-FROG traces the resulting pulse durations and the use of a fast Fourier transform (FFT) an estimation of the resulting pulse duration, at the individual cut-off wavelengths, was made. For the free-space stretcher this is depicted in a). For the fiber stretcher, the GDD and TOD of the fiber was taken into account to calculate the pulse durations, which are displayed in b).
In d) of figure 4.3, the pulse durations of the free-space stretcher, were plotted against the cut-off wavelengths. Panel e) shows the same plot for the pulse durations versus the cut-off wavelength of the fiber stretcher. For the free-space section of the stretcher, as well as for the fiber stretcher (4.3 a) b)) , a cut-off at higher wavelengths, between 1100 nm and 1090 nm, which responds to the low intensity tail of the spectrum, has negligible influence on the pulse duration. The root mean square width (RMS) of the pulse duration for the free-space section lies at 2.8 ps. The RMS value for the fiber stretcher is 110 ps at this spectral tuning point.
Further decreasing the cut-off wavelength stepwise from 1080 nm to 1060 nm, resembling the high intensity peak of the spectrum, leads to a clearly linear decrease of the pulse duration, seen at the RMS and FWHM values, and aat the bsolute pulse duration. The fiber stretcher also shows a decrease in pulse duration, but compared to the free-space stretcher less steeply. This happens mainly because the part in the spectrum with the highest intensity gets cut off.
When further cropping the spectrum, in the region of 1060 nm to 1040 nm, the pulse duration seems to increase again at the RMS-width and the FWHM level. This is mainly denoted to statistical errors in the data evaluation, since the main peak is cut off and the relative weight of the shorter peak has a bigger influence on the computation. A pure RMS evaluation of the pulse duration continues to show a decrease in pulse duration for both, the free-space stretcher as well as the fiber stretcher. Further cropping of the spectrum, to values below 1040 nm, leads to a

loss of the second peak of the spectrum, and therefore no significant evaluation can be made. In general, the pulse duration can be tailored to 3.5 ps - 2 ps pulses in the free-space section of the stretcher resulting in 120 ps to 50 ps pulses after the 110 m of fiber stretcher. The corresponding spectral tuning can be applied in the wavelength range starting from 1080 nm down to roughly 1040 nm, yielding a 40 nm bandwidth, continuous tuning range.

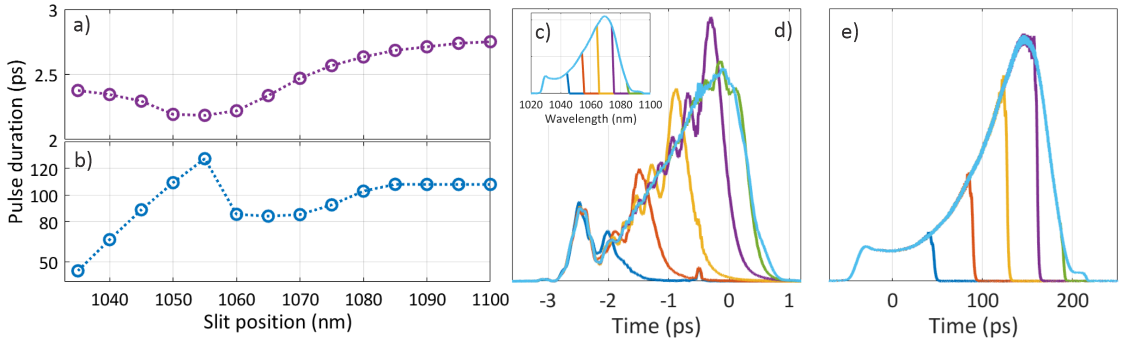

Figure 4.3: a) shows the pulse duration at the RMS level after the free-space stretcher and b) after 110 m of fiber stretcher, both, at different cut-off wavelengths by the slit type aperture. The small panel c) shows the spectra at different tuned wavelengths. d) shows the pulse durations after the free-space stretcher and e) after the fiber stretcher according to the cropped off wavelength. Reprinted with permission of Valentina Shumakova [44].

4.3.2 Pre-amplifier

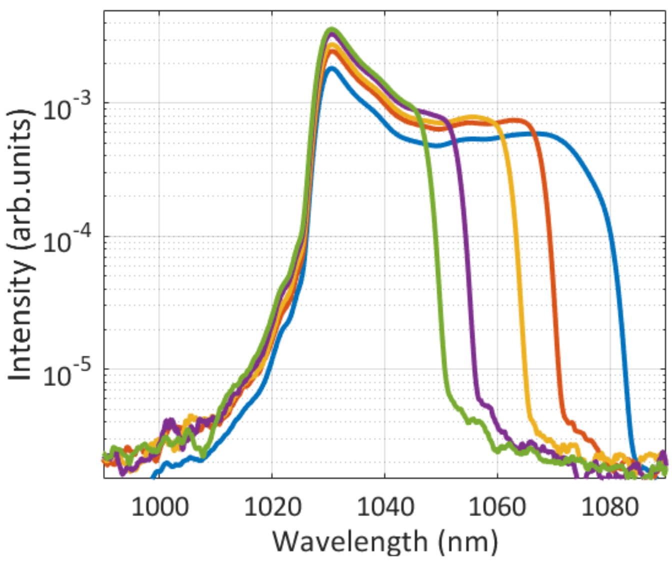

Figure 4.4: Spectra after amplifying with the pre amplification stage to a maximum average power of 265 mW, at different cut-off slit positions, normalized to the integrated area. The spectra were measured with an Ando Yokogawa AQ6315A OSA. Reprinted with permission of Valentina Shumakova [44].

Figure 4.4 shows the spectra of the pre-amplifier at different slit positions and different pump powers. The spectra were measured by an Ando Yokogawa AQ6315A OSA. Resulting from the low noise oscillator state a broadband spectrum with a bandwidth of 60 nm is measured. The center of gravity for the spectrum lies outside of the Yb gain maximum at 1075 nm. Through the

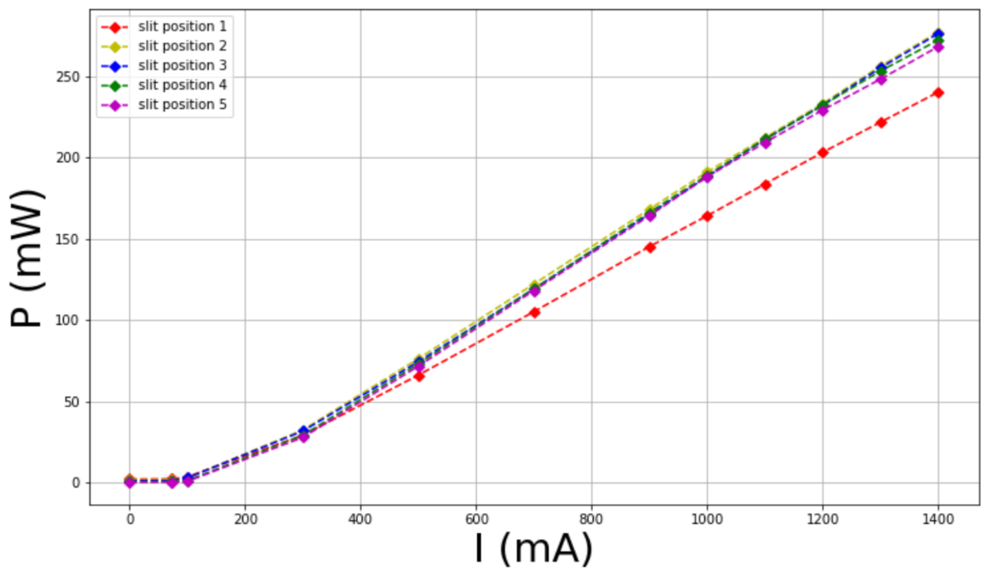

Figure 4.5: Shows different power slopes at the different slit positions tuning the spectra, according to 4.4

amplification the Yb gain maximum rises, shifting the center of gravity to the Yb gain maximum at 1040 nm. By using narrower slit positions the side peak at 1085 nm can be tuned and cropped off step wise such that it is making a visualization of the Yb gain maximum more clear. Starting at pump currents of around 800 mA a sharp maximum at 976 nm arises which is assigned to unabsorbed pump light of the pump diode. For evaluating the output power, and therefore plotting the power slope of the first stage, the unabsorbed pump light has to be taken into account. The average power values for the pre-amplification stage are measured by integrating the spectra measured by the OSA, in the 60 nm bandwidth region from 1000 nm to 1100 nm. It is important, that the unabsorbed pump light is left out for this evaluation since it does not contribute to the spectrum. Since the pre amplification stage is directly coupled to the first high power stage, it is not possible to measure the output power levels in free-space, without any alteration by contributions of the unabsorbed pump or absorption through the gain material of the first high power stage.

Figure 4.6 shows the power slope for the pre-amplification stage with the contribution of the unabsorbed pump and without the contribution of the unabsorbed pump. Starting from around 800 to 900 mA of pump current an influence of the unabsorbed pump can be observed. 4.5 shows the power slopes for different slit position, tuning the spectrum down to around 1050 nm (slit position 5). Except for slit position 1 all the power slopes show the same values and behaviour. Slight discrepancy between each individual slit position can be seen, which is resulting from a stepwise partial cropping of the peak centered at 1075. The maximum average output power for the pre-amplification stage lies at 265 mW at a pump power of 750 mW leaving a conversion efficiency of 35 %. When the unabsorbed pump of the pump diode is considered the conversion efficiency drops to 32 %. Nevertheless, the pre-amplification stage is getting saturated as can be seen in the figure 4.6, as the power slope declines from a linear behaviour at high pump powers. This holds true for both, the amplification without the slit type aperture placed inside the free-space section of the Martinez stretcher, as well as for the frequency tuned spectra. Measuring the power slopes at different slit position displays an arbitrarily spectral tuning down to 1050 nm to a bandwidth of about 25 nm, without disturbing the performance of the pre-amplification stage.

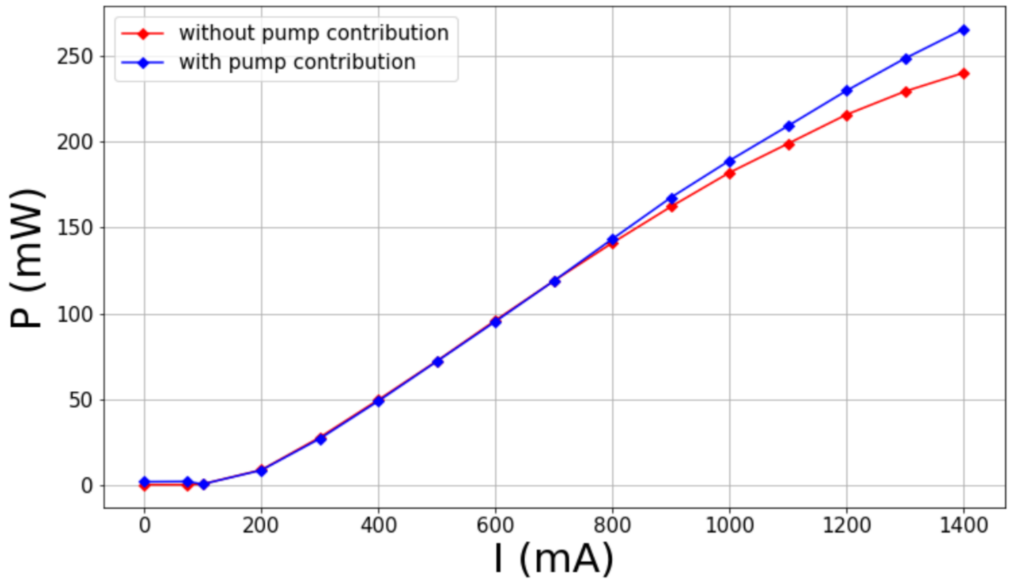

Figure 4.6: Shows the power slope for the pre amplifier with (blue) and without (red) contribution of the unabsorbed pump light. For the evaluation, the spectra at every pump current were taken and integrated for its power values.

4.3.3 First Power Stage - Double clad (DC) Amplifier

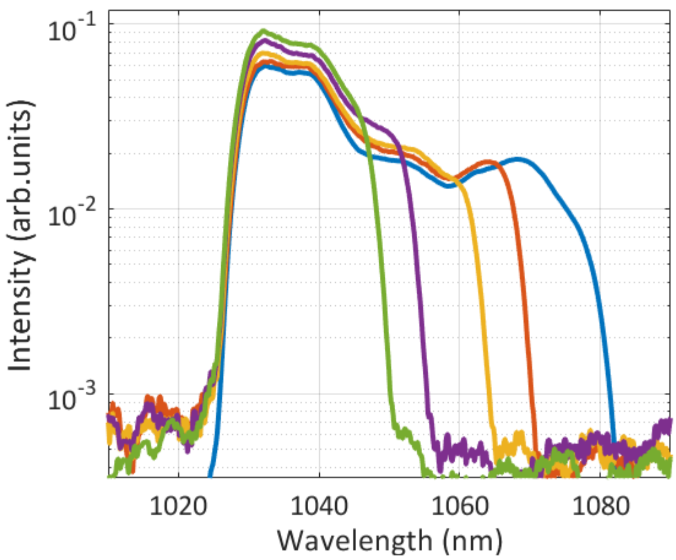

Figure 4.7: Spectra after amplifying with the first, power amplification stage to a maximum average power of 9 W at different cut-off slit positions, normalized to the integrated area. The spectra were measured with an Ando Yokogawa AQ6315A OSA. Reprinted with permission of Valentina Shumakova [44].

The first power amplification stage (using a LMA DC gain fiber) conserves the tuning abilities already observed in the pre-amplification stage. The different spectra for different slit positions were measured by the same OSA as in section 4.3.2 and are displayed in figure 4.7. A further rise of the Yb gain maximum, which holds the most PSD, can be seen. During the amplification

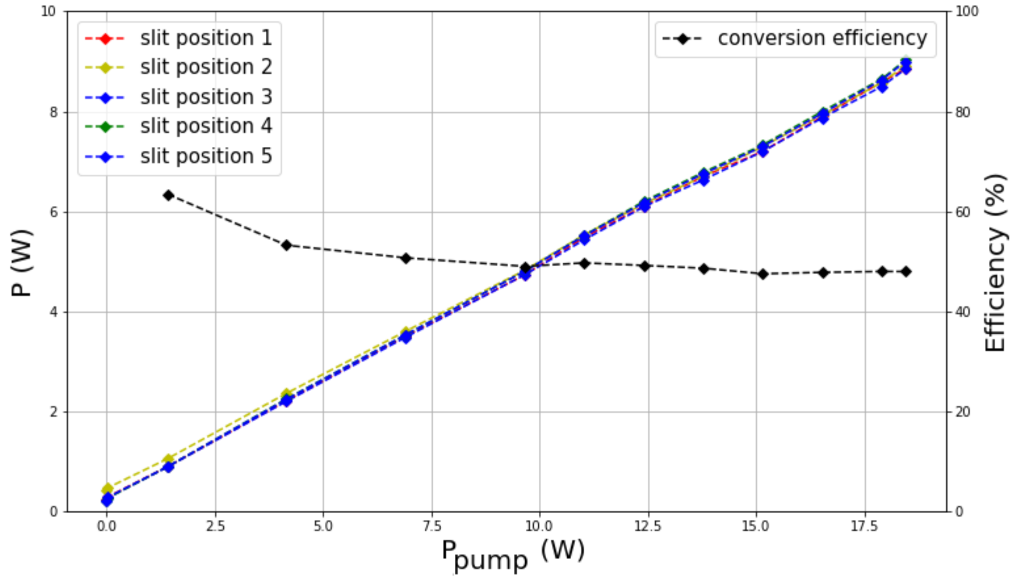

Figure 4.8: Shows the power slopes at different slit positions according to the spectral tuning. In black the conversion efficiency is shown.

process the spectra do not show any distortions by nonlinear effects like SPM, stimulated Raman scattering (SRS), self-steepening or any other kind of distortions.
The power slopes for this amplification stage are shown in 4.8 for the case of the slit aperture fully opened (slit position 1) and for the maximum narrowing (slit position 5) before the spectrum gets to narrow to be amplified effectively. In contrast to the pre amplification stage the output powers were measured in free-space with a thermal powermeter head (Thorlabs s322C). This is possible since the residual light of the unabsorbed pump is filtered out by a dichroic mirror directly after the output facet of the fiber. As can be seen in the two extreme cases of different power slopes (slit position 1 and 5), the spectral tuning does not influence the performance of the DC amplifier. The resulting measurements have, in the scope of the accuracy of the measurement, identical power slopes and the same maximum average output power at maximum pump power. Minor deviations in power levels are contributed to thermalisation effects of the used powermeter head. The maximum average output power is 9 W at a pump power of 18.5 W (corresponding to a pump current of 7.22 A). The resulting conversion efficiency at maximum average output power lies at 47 %. The conversion efficiencies at different pump powers are also displayed in 4.8. The first few data points are left out, since they are too close to the lasing threshold, to give reliable data.

4.3.4 Second Power Stage - ROD Fiber

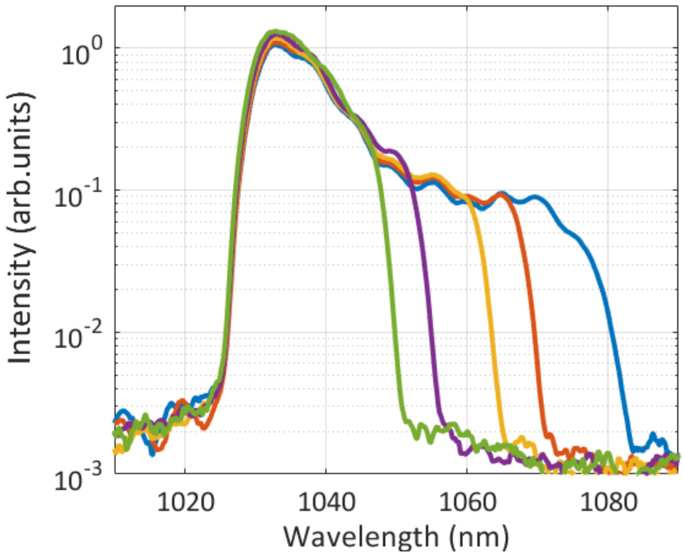

Figure 4.9: Spectra after amplifying with the second power amplification stage to a maximum average power of 100 W, at different cut-off slit positions, normalized to the integrated area. The spectra were measured with an Ando Yokogawa AQ6315A OSA Reprinted with permission of Valentina Shumakova [44].

.

Similarly to the DC amplifier, the second power amplification stage (ROD fiber), does not show any forms of nonlinearities in the measured spectra (measured with the same Ando Yokogawa OSA as in section 3.2). For the different slit positions, the spectral tuning is conserved. Figure 4.9 shows resulting spectra for different spectral tuning positions of the slit type aperture.

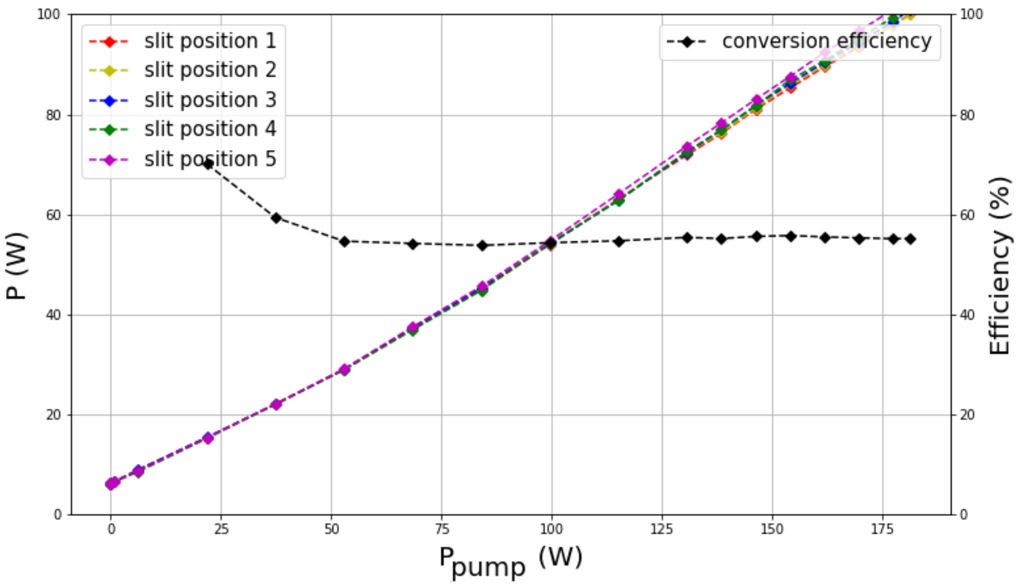

Figure 4.10: Power slopes at different slit positions of the second, power amplification stage are shown. In black the conversion efficiency, measured at different pump powers, is displayed.

For measuring the output power values the same thermal powermeter head as for the first power amplification stage 4.3.3 (Thorlabs Sc322) was used. The measured power slopes for different spectral tuning modulations are displayed in figure 4.10. It can be observed that different modulations of the input spectrum, by tuning the slit-type aperture, do not sustainably change the performance of the amplification stage. Minor modifications are mainly attributed to thermalisation effects resulting from the used power-meter head. The maximum average output power is 100 W at a pump power of 180 W (corresponding to a pump current of 22 A). This leads to a conversion efficiency of 54 % which is achieved regardless of the spectral tuning. The conversion efficiency at different pump powers is also displayed in 4.10. Again, the first few data points are left out, since they lie to close to the lasing threshold.

4.3.5 Grating Compressor

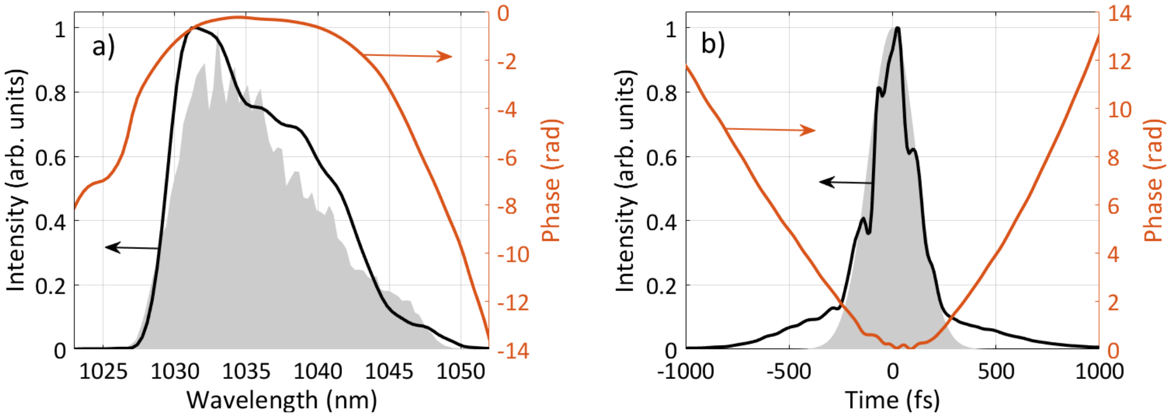

Figure 4.11: a) shows the spectrum after the grating compressor. The grey shaded area shows the spectrum measured retrieved from a SHG-FROG measurement, the black line is the spectrum measured with an OSA, the orange line the retrieved phase. b) shows the temporal shape of a pulse after compression. Reprinted with permission of Valentina Shumakova [44].

After the amplifier, the pulse train is expanded by a factor of 3 by the telescope discussed in section 4.2.2. Through the isolator, protecting the ROD fiber from back reflections, additionally 4 % of power, resulting in ultimately 96 W average output power, are lost. The grating compressor is placed yielding a near maximum efficiency of 96 % per grating. Four a double pass through the compressor 79 % efficiency are achieved, resulting in a average power of 80 W after the compressor.
The resulting pulse duration after the CPA at minimum grating distance is 230 fs. This pulses still have linear positive chirp. To get the pulse to it's transform limited pulse durations, further dispersion management of the HOD is needed. The estimated transform limited minimum supported pulse duration is ∼65 fs. The measurements of the pulse duration were done by a SHG-FROG and are shown in figure 4.11. Further investigation of the SHG-FROG measurement shows that the temporal envelope has a smooth Gaussian profile with ∼ 90 % of the power inside the main peak. The spectrum seen in a) shows good agreement with the simulated data and no further distortions are attributed by the grating compressor.

4.3.6 Beam Quality

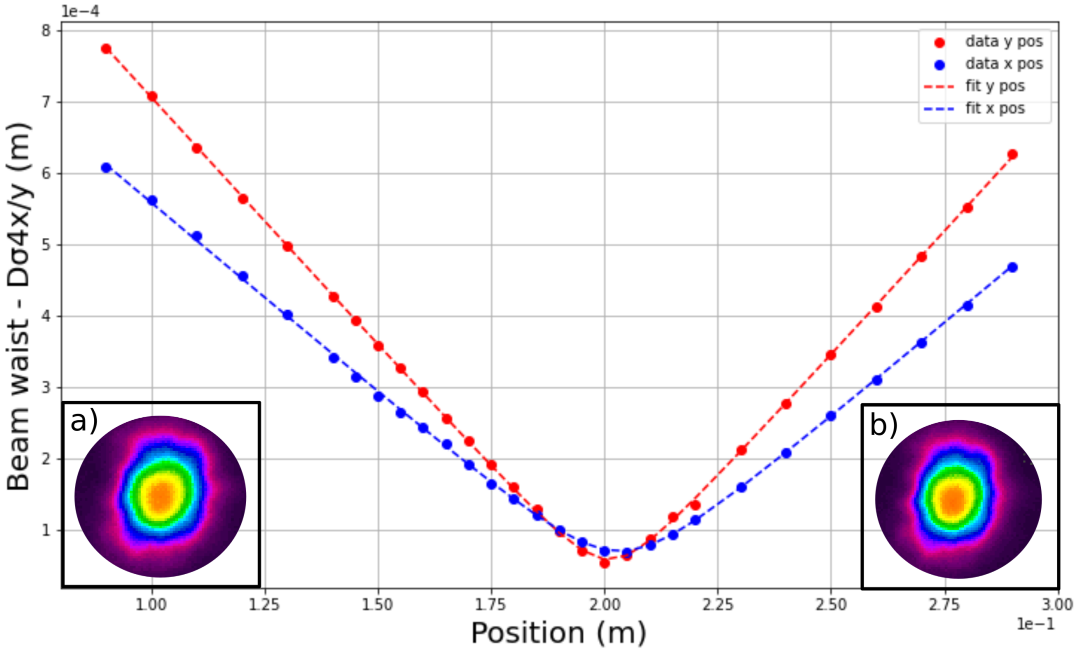

Figure 4.12: The figure shows the fit and data for the M^2 values is x direction (blue) and y direction (red) directly after the ROD fiber without a beam expander. Panel a) shows the beam at slit position 1 (no spectral tuning), b) shows the beam at slit position 5 (maximum spectral tuning)

Evaluating the M^2 factor, after the amplification stages without the telescope in the setup shows a beam with an M_x^2 of 1.07 and M_y^2 of 1.11, which is in good agreement with the specified values of ≤ 1.3, provided by the manufacturer of the ROD fiber. However, placing the beam expander telescope (4.2.2) f_1 =-100, f_2 =300, a degradation of the M^2 values of about 0.1 for the y direction, to 1.2 can be seen. The fits for the M squared values, measured directly after the ROD fiber, can be seen in figure 4.12. After the grating compressor, the measured M^2 factors are in good agreement with the values measured directly after the amplifier, with and without the beam expander, respectively. In total after compressing the beam, at the current work point a M^2 value of 1.05 in x direction of the beam waist and a value of 1.22 in y direction of the beam waist is measured.
The measurements were done using a focussing lens with a focal length of $f = 50$ mm, and a silicon charge-coupled device (CCD) beam profiler camera (Newport: LBP2-HR-VIS2), providing the beam diameters. The fit was done using the function of *Siegmann et al.* [45]:

$$\omega^2(z) = \omega_0^2 + M^4(\frac{\lambda}{2\pi\omega_0^2})(z - z_0)^2 \tag{4.1}$$

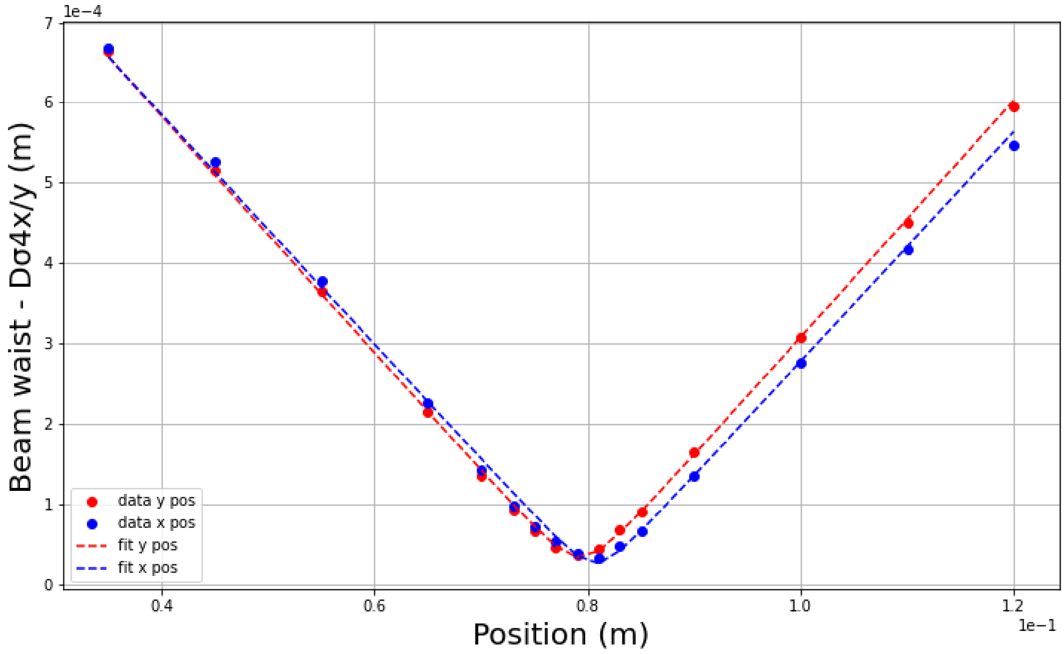

Figure 4.13: The figure shows a detailed M^2 measurement of the final beam. Blue line and points denote to the x direction of the beam waist, red points and lines to the y direction.

Additionally, seen in 4.12 a) is the beam without a beam expander directly after the amplification stage and b) the beam after propagating through the telescope. The beam shows no signs of spatial chirp or any kind of distortions. The beam intensity distribution in both, x and y direction show a Gaussian beam profile. Any distortions that can be seen in the beam profile are accounted to dirt on the used neutral density filters, protecting the beam profiler.

4.3.7 Noise Characterization

Phase Noise

The PN of the system was measured using a signal to source analyser (Rhode & Schwartz FSWP-8) with a frequency range from 1 MHz to 8 GHz. The pulse train was measured using an InGaAs photo-diode (Thorlabs DET08CL) with a 5 GHz bandwidth, which was connected by a 50-Ohm RF-terminator to the signal to source analyser. In order to avoid spatial noise, emerging at the detector facet, the beam was focused onto the detector chip. In addition to prevent saturation of the photo-diode, the beam has to be attenuated.
To characterize the phase noise a single side band measurement (SSB) with 2000 cross-correlations and a resolution bandwidth of 1 % was made. The measurement was made using the 15 th harmonic of the repetition rate. This is done, because the PSD is dependant by factor n^2, on the used harmonic of the repetition rate 2.5 and therefore leading to a n^2 times rise of the measured PSD level. Afterwards the measurement has to be renormalized again to evaluate the PN on the actual noise level, according to the first harmonic. With this, the shot-noise level of the detector, which corresponds to the least measured PN introduced through a single photon, is lowered.
Figure 4.14 shows the PN noise-plot for the oscillator (black), the amplification system after the last power stage without (blue), and with (green) spectral tuning. Comparing the three curves shows, that the PN from the laser oscillator is conserved in the CPA system. Moreover, comparing the blue and the green curve, it becomes clear, that spectral tuning does not introduce

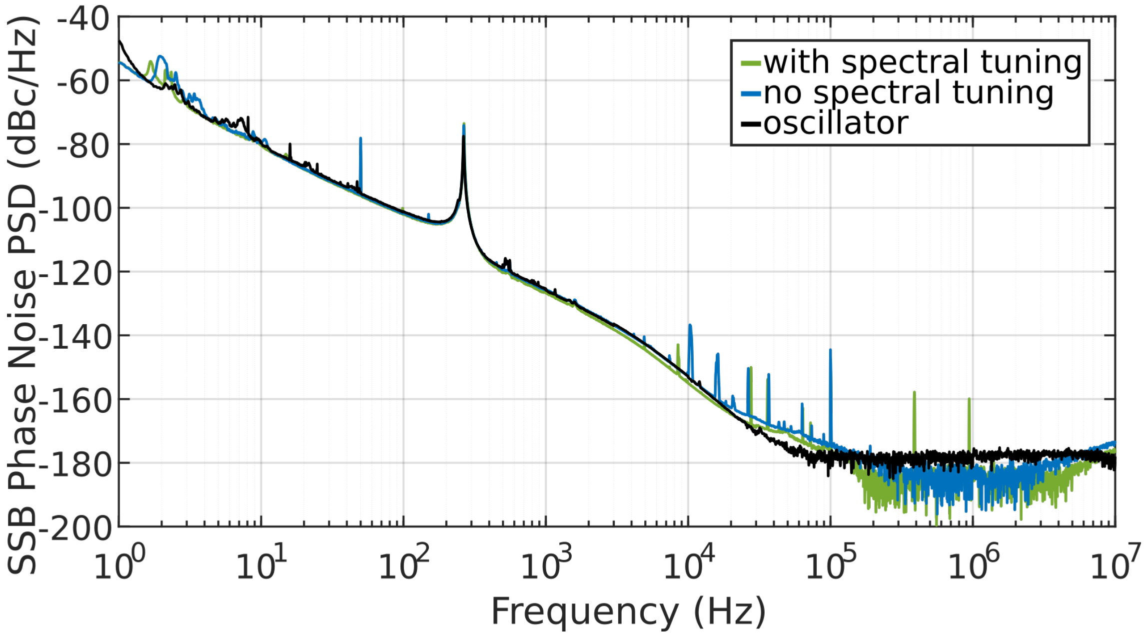

Figure 4.14: Shows the SSB measurement of the phase noise. The green curve resembles the 100 W average power beam with spectral tuning, the blue curve without spectral tuning. The black curve is the Pn of the oscillator. Reprinted with permission of Valentina Shumakova [44].

further PN to the system. Deviations in the blue and green curve emerging in the region from 10^0 - 10^1 Hz, originate from low averaging times. At 120 Hz a prominent peak can be seen in all noise measurements. This peak is attributed to the relaxation of the Yb:gain medium. At 14 kHz the black curve, of the laser oscillator, reaches the shot-noise level. The two plots for the amplifier system reach their shot-noise level at around 100 kHz. This was expected, since the measurements on the amplified pulse train have a higher average power and are thus rising the shot-noise level since the single photon has more energy at higher amplifications than for the oscillator. Therefore deviations between 10^4 and 10^5 Hz are uncertainties in the measuring method. The delta like peaks in this region are mainly attributed to radiofrequency (RF) disturbances.

Relative Intensity Noise

The measurement of the RIN was done using the same signal to source analyser as for the PN. The used detector is a Si diode (Thorlabs PDA-36A-EC), where the internal gain was set to 0 dB. The measurement technique used is a baseband measurement with 10 MHz (f_{3dB} bandwidth, 200 cross-correlations, and a resolution bandwidth of 1 %. By focussing the beam on the diode-chip spatial disturbances are avoided. Figure 4.15 shows the RIN measured for the system. The grren curve shows the RIN of the beam with spectral tuning after amplification, the blue curve is the noise curve for amplification without spectral tuning, and the purple curve shows the noise curve for the pump diode for the last amplification stage. The higher frequencies, $>$100 kHz were excluded from the measurement, since several measurements at different incident powers showed, that the PSD in this frequency region depends on the incident power. Therefore the measured RIN is seen as a measuring artefact resulting from the used detector. In low frequency regions (4.15 region I, frequencies 10^0-10^1) the noise for both, the amplification with and without spectral tuning, show a deviation from the pump diode. These deviations are mainly contributed to mechanical noise picket up in the laser system. After that, in region II (10^1 to $5 * 10^4$) the RIN of the amplifier system is dominated by the fluctuations of the pump diode. This behaviour was expected, since we saturate our gain fibers and is described in exact detail by *Tünnermann et al.* [55]. At 50 kHz (region III), the roll-off frequency is reached. From this frequency region on to

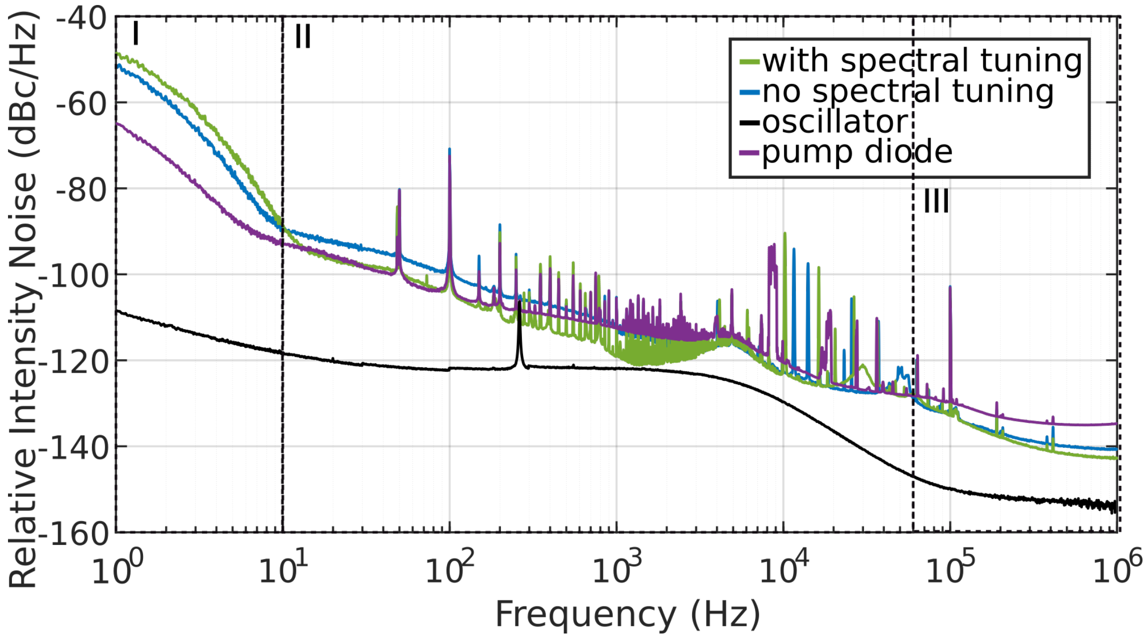

Figure 4.15: The RIN measured for the full spectrum (blue), the tuned spectrum (green) at 100 W average output power. The RIN of the pump diode is pictured in purple and in black for comparison the RIN of the oscillator is shown. Reprinted with permission of Valentina Shumakova [44].

10^6 (region III) in the plot the RIN is dominated by the fluctuations of the seed signal. Again this behaviour was expectad as described in [55]. Any fluctuations between the noise curve with spectral tuning and without spectral tuning result from uncertainties in the measurement.

Chapter 5

Conclusion and Outlook

We used a homebuilt low noise figure-9 oscillator as seed laser for the CPA system. Based on the findings of *Mayer et al.* this seed laser is tuned to operate in a low noise state yielding narrow linewidths. The seed oscillator was characterized for it's spectral, temporal, and noise properties. The main part of this thesis deals with development and characterization of a high average power CPA. Based on the characterization of the seed laser a suitable stretching scheme, with additionally continuous spectral tuning, was applied.

The CPA is designed to yield high average powers and at the same time, conserve the low PN and narrow linewidths of the seed oscillator and operate in the lowest possible RIN regime. The grating compressor compresses the pulses to the femtosecond level. After compression a detailed pulse characterization including the temporal and spectral properties of the pulses, RIN and PN properties as well as an evaluation of the beam quality was performed. With the chosen design criteria of the amplifier system, an efficient parametric conversion to the mid-IR and subsequent use of the OFC for precision spectroscopy is guaranteed.

The pulses from the oscillator have enough power to saturate the pre-amplification stage. From the power slopes, a saturation of the first and the second power amplification stages can be seen. The system produces the expected pulse train with 100 W average power, with a pulse duration after compression of nearly bandwidth limited 230 fs. Furthermore, the spectral tuning, does not degrade the power performance of the system.

The slit-type aperture in the Martinez stretcher, shows sustainable spectral tuning in a range of 65 nm. By cropping the spectra in the given range, the power performance of the system is not significantly affected and the gain material at every amplification stage is saturated. Minor deviations, at different slit positions, are denoted to measurement artefacts like the thermalisation of the thermal powermeter head.

The system has a state of the art low noise performance. The measurements of the RIN show that the governing factor for the RIN is the pump diode. This was expected, as we know from [55] and since at every slit position, every amplification stage is saturated. Measurements of the PN show that it is conserved throughout all amplification stages. Minor deviations seen, are denoted to a difference in averaging time or a difference in average power.

For both, the PN and the RIN, the slit type aperture does not depict an additional noise source. The RIN and PN properties are conserved through spectral tuning.

After the amplification, the beam quality measurements with a CCD camera show no signs of spatial chirp, yielding a clean propagation of the light through the stretcher, amplification stages and grating compressor. The final M^2 beam quality measurements, yield a M^2 factor of $\mathrm{M}_x^2 = 1.05$ and $\mathrm{M}_y^2 = 1.22$, which is in agreement, with the provided data of the manufacturer of the third stage amplifier gain fiber.

The compressed narrowband pulses of 230 fs, with a peak power of ($\sim$ 2 MW) are suitable as pump for high efficiency in optical parametric conversion stages and subsequent use in precision

spectroscopy. With the high power pulses and low noise operation, the system depicts an ideal candidate for the proposed application for precision spectroscopy in the mid-IR.
Therefore, next steps will be applying an active stabilization schema (f_{rep} and f_{CEO}) to the ML femtosecond laser to use it as an OFC. For this purpose, a first CEO frequency has already been measured successfully. Afterwards, an optical parametric oscillator stage to convert to the mid-IR wavelength region and an optical parametric amplification stage to amplify the mid-IR signals are planned. Afterwards, an enhancement cavity to induce the interaction of light with the first probe-gas is planned. The measurement device will be an Fourier Transform Spectrometer, which is currently characterized and designed.

Bibliography

[1] Félicie Albert, M E Couprie, Alexander Debus, Mike C Downer, Jérôme Faure, Alessandro Flacco, Leonida A Gizzi, Thomas Grismayer, Axel Huebl, Chan Joshi, M Labat, Wim P Leemans, Andreas R Maier, Stuart P D Mangles, Paul Mason, François Mathieu, Patric Muggli, Mamiko Nishiuchi, Jens Osterhoff, P P Rajeev, Ulrich Schramm, Jörg Schreiber, Alec G R Thomas, Jean-Luc Vay, Marija Vranic, and Karl Zeil. 2020 roadmap on plasma accelerators. *New Journal of Physics*, 23(3):031101, mar 2021.

[2] Zhenao Bai, Zhenxu Bai, Xiaolong Sun, Yong Liang, Kun Wang, Duo Jin, and Zhongwei Fan. "A 33.2 W High Beam Quality Chirped-Pulse Amplification-Based Femtosecond Laser for Industrial Processing. *Materials*, 13:2841, 06 2020.

[3] Giulio Cerullo and Sandro De Silvestri. Ultrafast optical parametric amplifiers. *Review of Scientific Instruments*, 74(1):1–18, 2003.

[4] Guoqing Chang and Zhiyi Wei. Ultrafast Fiber Lasers: An Expanding Versatile Toolbox. *iScience*, 23(5):101101, 2020.

[5] Kevin C. Cossel, Eleanor M. Waxman, Ian A. Finneran, Geoffrey A. Blake, Jun Ye, and Nathan R. Newbury. Gas-phase broadband spectroscopy using active sources: progress, status, and applications [Invited]. *J. Opt. Soc. Am. B*, 34(1):104–129, Jan 2017.

[6] G. D. Dickenson, M. L. Niu, E. J. Salumbides, J. Komasa, K. S. E. Eikema, K. Pachucki, and W. Ubachs. Fundamental Vibration of Molecular Hydrogen. *Physical Review Letters*, 110(19), may 2013.

[7] M. L. Diouf, F. M. J. Cozijn, K.-F. Lai, E. J. Salumbides, and W. Ubachs. Lamb-peak spectrum of the HD (2-0) P(1) line. *Phys. Rev. Research*, 2:023209, May 2020.

[8] N. J. Doran and David Wood. Nonlinear-optical loop mirror. *Opt. Lett.*, 13(1):56–58, Jan 1988.

[9] I.N. Duling. Subpicosecond all-fibre erbium laser. *Electronics Letters*, 27:544–545(1), March 1991.

[10] Patrick Dupré. Hyperfine transitions in the first overtone mode of hydrogen deuteride. *Phys. Rev. A*, 101:022504, Feb 2020.

[11] Jakob Fellinger. *Versatile and robust Yb:fiber lasers for single and dual-comb applications*. Wien, 2020.

[12] Jakob Fellinger, Georg Winkler, P. E. Collin Aldia, Aline S. Mayer, Valentina Shumakova, Lukas W. Perner, Vito F. Pecile, Tadeusz Martynkien, Pawel Mergo, Grzegorz Soboń, and Oliver H. Heckl. Simple approach for extending the ambiguity-free range of dual-comb ranging. *Opt. Lett.*, 46(15):3677–3680, Aug 2021.

[13] M. E. Fermann, F. Haberl, M. Hofer, and H. Hochreiter. Nonlinear amplifying loop mirror. *Opt. Lett.*, 15(13):752–754, Jul 1990.

[14] I.E. Gordon, L.S. Rothman, C. Hill, R.V. Kochanov, Y. Tan, P.F. Bernath, M. Birk, V. Boudon, A. Campargue, K.V. Chance, B.J. Drouin, J.-M. Flaud, R.R. Gamache, J.T. Hodges, D. Jacquemart, V.I. Perevalov, A. Perrin, K.P. Shine, M.-A.H. Smith, J. Tennyson, G.C. Toon, H. Tran, V.G. Tyuterev, A. Barbe, A.G. Császár, V.M. Devi, T. Furtenbacher, J.J. Harrison, J.-M. Hartmann, A. Jolly, T.J. Johnson, T. Karman, I. Kleiner, A.A. Kyuberis, J. Loos, O.M. Lyulin, S.T. Massie, S.N. Mikhailenko, N. Moazzen-Ahmadi, H.S.P. Müller, O.V. Naumenko, A.V. Nikitin, O.L. Polyansky, M. Rey, M. Rotger, S.W. Sharpe, K. Sung, E. Starikova, S.A. Tashkun, J. Vander Auwera, G. Wagner, J. Wilzewski, P. Wcisło, S. Yu, and E.J. Zak. The HITRAN2016 molecular spectroscopic database. *Journal of Quantitative Spectroscopy and Radiative Transfer*, 203:3–69, 2017. HITRAN2016 Special Issue.

[15] Theodor W. Hänsch. Nobel Lecture: Passion for precision. *Rev. Mod. Phys.*, 78:1297–1309, Nov 2006.

[16] Wolfgang Hänsel, Heinar Hoogland, Michele Giunta, Sebastian Schmid, Tilo Steinmetz, Ralf Doubek, Peter Mayer, Sven Dobner, Carsten Cleff, Marc Fischer, and Ronald Holzwarth. *All Polarization-Maintaining Fiber Laser Architecture for Robust Femtosecond Pulse Generation*, pages 331–340. 01 2018.

[17] Tongxiao Jiang, Yifan Cui, Pei Lu, Chen Li, Aimin Wang, and Zhigang Zhang. All PM Fiber Laser Mode Locked With a Compact Phase Biased Amplifier Loop Mirror. *IEEE Photonics Technology Letters*, 28(16):1786–1789, 2016.

[18] Jungwon Kim and Youjian Song. Ultralow-noise mode-locked fiber lasers and frequency combs: principles, status, and applications. *Adv. Opt. Photon.*, 8(3):465–540, Sep 2016.

[19] Fritz Kurt Kneubühl and Markus Werner Sigrist. *Prinzip der Laser*, pages 39–56. Vieweg+Teubner Verlag, Wiesbaden, 1999.

[20] N. Kuse, J. Jiang, C.-C. Lee, T. R. Schibli, and M.E. Fermann. All polarization-maintaining Er fiber-based optical frequency combs with nonlinear amplifying loop mirror. *Opt. Express*, 24(3):3095–3102, Feb 2016.

[21] Xinlong Li, Melanie A. R. Reber, Christopher Corder, Yuning Chen, Peng Zhao, and Thomas K. Allison. High-power ultrafast Yb:fiber laser frequency combs using commercially available components and basic fiber tools. *Review of Scientific Instruments*, 87(9):093114, 2016.

[22] Hong Lin, D.K. Donald, and W.V. Sorin. Optimizing polarization states in a figure-8 laser using a nonreciprocal phase shifter. *Journal of Lightwave Technology*, 12(7):1121–1128, 1994.

[23] Guanyu Liu, Xinghe Jiang, Aimin Wang, Guoqing Chang, Franz Kaertner, and Zhigang Zhang. Robust 700 MHz mode-locked Yb:fiber laser with a biased nonlinear amplifying loop mirror. *Opt. Express*, 26(20):26003–26008, Oct 2018.

[24] Wu Liu, Haosen Shi, Jiahua Cui, Chen Xie, Youjian Song, Chingyue Wang, and Minglie Hu. Single-polarization large-mode-area fiber laser mode-locked with a nonlinear amplifying loop mirror. *Opt. Lett.*, 43(12):2848–2851, Jun 2018.

[25] Daping Luo, Yang Liu, Chenglin Gu, Chao Wang, Zhiwei Zhu, Wenchao Zhang, Zejiang Deng, Lian Zhou, Wenxue Li, and Heping Zeng. High-power Yb-fiber comb based on pre-chirped-management self-similar amplification. *Applied Physics Letters*, 112(6):061106, 2018.

[26] C.P.K. Manchee, J. Möller, and R.J.D. Miller. Highly stable, 100 W average power from fiber-based ultrafast laser system at 1030 nm based on single-pass photonic-crystal rod amplifier. *Optics Communications*, 437:6–10, 2019.

[27] O. E. Martínez. 3000 times grating compressor with positive group velocity dispersion: Application to fiber compensation in 1.3-1.6 μm region. *IEEE Journal of Quantum Electronics*, 23:59–64, 1987.

[28] O. E. Martinez, J. P. Gordon, and R. L. Fork. Negative group-velocity dispersion using refraction. *J. Opt. Soc. Am. A*, 1(10):1003–1006, Oct 1984.

[29] V.J. Matsas. Selfstarting passively mode-locked fibre ring soliton laser exploiting nonlinear polarisation rotation. *Electronics Letters*, 28:1391–1393(2), July 1992.

[30] A. Mayer. Leveraging Novel Nonlinear Devices for Compact Gigahertz Frequency Combs. 2018.

[31] Aline S. Mayer, Wilfrid Grosinger, Jakob Fellinger, Georg Winkler, Lukas W. Perner, Stefan Droste, Sarper H. Salman, Chen Li, Christoph M. Heyl, Ingmar Hartl, and Oliver H. Heckl. Flexible all-PM NALM Yb:fiber laser design for frequency comb applications: operation regimes and their noise properties. *Opt. Express*, 28(13):18946–18968, Jun 2020.

[32] J. W. Nicholson and M. Andrejco. A polarization maintaining, dispersion managed, femtosecond figure-eight fiber laser. *Opt. Express*, 14(18):8160–8167, Sep 2006.

[33] R. Paschotta. Amplified Spontaneous Emission, [Online]. *RP Photonics Encyclopedia, Available at:* $https://www.rp-photonics.com/amplified_spontaneous_emission.html$ *,(last visited on* $20.07.2022$*).*

[34] R. Paschotta. Fiber Amplifiers , [Online]. *RP Photonics Encyclopedia, Available at:* $https://www.rp-photonics.com/fiber_amplifiers.html$ *,(last visited on* $16.08.2022$*).*

[35] R. Paschotta. Gain Saturation, [Online]. *RP Photonics Encyclopedia, Available at:* $https://www.rp-photonics.com/gain_saturation.html$ *,(last visited on* $01.06.2022$*).*

[36] R. Paschotta. Laser Noise, [Online]. *RP Photonics Encyclopedia, Available at:* $https://www.rp-photonics.com/laser_noise.html$ *,(last visited on* $01.06.2022$*).*

[37] R. Paschotta. Chromatic Dispersion, [Online]. *RP Photonics Encyclopedia, Available at:* $https://www.rp-photonics.com/chromatic_dispersion.html$*, (last visited on* $01.06.2022$*)*, October 2008.

[38] Rüdiger Paschotta. Noise of mode-locked lasers (Part I): Numerical model. *Applied Physics B*, 79:153–162, 07 2004.

[39] Rüdiger Paschotta. Noise of mode-locked lasers (Part II): Timing jitter and other fluctuations. *Applied Physics B*, 79:163–173, 07 2004.

[40] Nathalie Picque and Theodor W. Haensch. Frequency comb spectroscopy. *Nature photonics*, 13(3):146–157, 2019.

[41] Enrico Rubiola and Francois Vernotte. The Companion of the Enrico's Chart for Phase Noise and Two-Sample Variances, 2022.

[42] D.N. Schimpf, D. Müller, S. Hädrich, T. Schreiber, J. Limpert, and A. Tünnermann. Control of Nonlinearity in Fiber CPA System by Pulse-shaping. In *Advanced Solid-State Photonics*, page TuC2. Optica Publishing Group, 2007.

[43] E. Shestaev, S. Hädrich, N. Walther, T. Eidam, A. Klenke, I. Seres, Z. Bengery, P. Jójárt, Z. Várallyay, Á. Börzsönyi, and J. Limpert. Carrier-envelope offset stable, coherently combined ytterbium-doped fiber CPA delivering 1 kW of average power. *Opt. Lett.*, 45(23):6350–6353, Dec 2020.

[44] Valentina Shumakova, Vito F. Pecile, Jakob Fellinger, Michael Leskowschek, P. E. Collin Aldia, Aline S. Mayer, Lukas W. Pernera, Sarper Salman, Mingqi Fan, Prannay Balla, Stéphane Schilt, Christoph M. Heyl, Ingmar Hartl, Gil Porat, and Oliver H. Heckl. Spectrally Tunable High Power Yb:fiber Chirped Pulse Amplifier. In preparation.

[45] A. E. Siegman. How to (Maybe) Measure Laser Beam Quality. In *DPSS (Diode Pumped Solid State) Lasers: Applications and Issues*, page MQ1. Optica Publishing Group, 1998.

[46] Abneesh Srivastava and Joseph T Hodges. Development of a High-Resolution Laser Absorption Spectroscopy Method with Application to the Determination of Absolute Concentration of Gaseous Elemental Mercury in Air. *Analytical chemistry*, 90(11):6781—6788, June 2018.

[47] Donna Strickland and Gerard Mourou. Compression of amplified chirped optical pulses. *Opt. Commun.*, 55(6):447–449, 1985. [Erratum: Opt.Commun. 56, 219–221 (1985)].

[48] B. E. A. Saleh & M. C. Teich. *Fundamental of Photonics*, chapter 3, pages 80–107. John Wiley & Sons, Ltd, 1991.

[49] B. E. A. Saleh & M. C. Teich. *Fundamental of Photonics*, chapter 13, pages 482–531. John Wiley & Sons, Ltd, 2007.

[50] B. E. A. Saleh & M. C. Teich. *Fundamental of Photonics*, chapter 22, pages 936–1015. John Wiley & Sons, Ltd, 2007.

[51] B. E. A. Saleh & M. C. Teich. *Fundamental of Photonics*, chapter 14, pages 532–566. John Wiley & Sons, Ltd, 2007.

[52] B. E. A. Saleh & M. C. Teich. *Fundamentals of Photonics*, chapter 5, pages 152–196. John Wiley & Sons, Ltd, 2007.

[53] B. E. A. Saleh & M. C. Teich. *Lasers*, chapter 16, pages 657–730. John Wiley & Sons, Ltd, 2019.

[54] E. Treacy. Optical pulse compression with diffraction gratings. *IEEE Journal of Quantum Electronics*, 5(9):454–458, September 1969.

[55] Henrik Tünnermann, Jörg Neumann, Dietmar Kracht, and Peter Weßels. Gain dynamics and refractive index changes in fiber amplifiers: a frequency domain approach. *Opt. Express*, 20(12):13539–13550, Jun 2012.

[56] Denis Villate, Nathalie Blanchot, and Claude Rouyer. Beam breakup integral measurement on high-power laser chains. *Opt. Lett.*, 32(5):524–526, Mar 2007.

[57] Yunzheng Wang, Liqiang Zhang, Zhuang Zhuo, and Songzhen Guo. Cross-splicing method for compensating fiber birefringence in polarization-maintaining fiber ring laser mode locked by nonlinear polarization evolution. *Appl. Opt.*, 55(21):5766–5770, Jul 2016.

[58] Xuan Xu, Fedor Rudakov, and Peter M. Weber. Chemical analysis from a distance: Spatially resolved, remote sensing using backward transient absorption. *Chemical Physics Letters*, 793:139435, 2022.

[59] Michalis N. Zervas. Transverse mode instability, thermal lensing and power scaling in Yb3+-doped high-power fiber amplifiers. *Opt. Express*, 27(13):19019–19041, Jun 2019.

[60] Jian Zhao, Wenxue Li, Chao Wang, Yang Liu, and Heping Zeng. Pre-chirping management of a self-similar Yb-fiber amplifier towards 80 W average power with sub-40 fs pulse generation. *Opt. Express*, 22(26):32214–32219, Dec 2014.

[61] A. M. Zheltikov. Understanding the nonlinear phase and frequency shift of an ultrashort light pulse induced by an inertial third-order optical nonlinearity. *Phys. Rev. A*, 79:023823, Feb 2009.

List of Figures

Abstract

Applications like remote sensing, ranging, chemical analysis in health and environmental sciences, or spectroscopy of extraterrestrial objects need precise and broadband spectroscopic databases to perform high-quality measurements. The mid infrared (mid-IR) wavelength range (2.5 - 20 μm) is of special interest since here fundamental molecular vibrations take place. However, acquiring high precision data at this wavelength range is challenging, and subject of ongoing research. To perform, precision spectroscopy in the mid-IR the molecular spectral lines need to be free of Doppler broadening. One way to achieve this is by saturating the spectral lines of the transitions with a laser.

During the years fiber lasers, generating an optical frequency comb (OFC), have emerged as a good possible source to perform precise measurements. The generated OFC yields narrow linewidths, and the laser can be tuned to be in a low noise operation mode. To get to mid-IR wavelengths, the spectrum provided by the fiber laser must be converted properly. Common methods for this are based on optical parametric conversion. However, to achieve an efficient light conversion and subsequently saturate the spectral lines the fiber laser doesn't yield high enough power. Therefore, a suitable amplification scheme, conserving narrow linewidths and low noise operation is needed. A common method for this purpose is chirped pulse amplification (CPA).

This thesis deals with the experimental development of a chirped pulse amplifier. The generated OFC is characterized for its spectral, and temporal properties during the amplification process. Furthermore, a detailed investigation to the noise and power properties with respect to the goal of conversion to the mid-IR and subsequent precision spectroscopy is done.

We were able, to show, that the generated OFC yields an average output power of 100 W at pulse durations of $\sim$230fs. Thus, being sufficient for an efficient frequency conversion. Moreover, the CPA system preserves the low phase noise (PN) properties of the seed laser at frequencies below 100 kHz, and exhibits lower amplitude noise than comparable laser systems. Thus, the generated system depicts an ideal light source for performing precision spectroscopy.

Zusammenfassung

Anwendungen wie zum Beispiel Fernerkundung, Entfernungsmessung, chemische Analysen im Bereich der Gesundheits- und Umweltwissenschaften oder spektroskopische Messungen von extraterrestrischen Objekten benötigen genaue breitbandige spektroskopische Datenbanken. Der Wellenlängenbereich des mittleren Infrarots ist dabei von besonderem Interesse, da in diesem Bereich fundamentale molekulare Übergänge stattfinden. Die Datenaufnahme für diese Übergänge ist jedoch keine einfache Aufgabe und ist daher Gegenstand aktueller Forschungsprojekt. Um Präzisionsspektroskopie im mittleren infrarot durchzuführen müssen diese Übergänge frei von Dopplerverbreiterung sein. Eine Möglichkeit für die Messungen ist es die Übergänge mit Laserlicht zu Sättigen.

Währen den letzten Jahrzehnten haben sich Faselaser, mit denen optische Frequenzkämme generiert werden können, als gutes Hilfsmittel füre diese Messungen herausgestellt. Der Frequenzkamm, der in solchen Lasern hergestellt wird, hat enge Linienbreiten. Man kann den Aufbau so anpassen, dass ein Frequenzkamm in einem Zustand mit geringem Hintergrundrauschen entsteht. Um den Frequenzkamm ins mittlere Infrarot zu verschieben muss das Spektrum angemessen konvertiert werden. Für gewöhnlich wird optische parametrische Konversion zur Frequenzverschiebung verwendet. Die Intensität des im Faserlaser produzierten Lichts reicht jedoch nicht aus um die nichtlinearen Prozesse, die für die Frequenzverschiebung verantwortlich sind, und gleichzeitig eine Sättigung der spektralen Übergänge, anzuregen. Deshalb benötigt man ein adäquates System mit dem man das Laserlicht verstärken kann und gleichzeitig die engen Linienbreiten und das geringe Hintergrundrauschen des Frequenzkammes erhalten werden. Eine weit verbreitete Methode dafür ist gechirpte Puls-Verstärkung (CPA).

Diese Masterarbeit behandelt den experimentellen Aufbau eines CPA. Der dort generierte Frequenzkamm wird auf seine spektralen und temporalen Eigenschaften, während der Verstärkung charakterisiert. Des Weiteren werden das Hintergrundrauschen und die Leistungsseigenschaften des Frequenzkammes bezüglich des Ziels, der Frequenzverschiebung und anschließenden Präzisionsspektroskopie, untersucht.

Mit den Messungen konnte gezeigt werden, dass der generierte Frequenzkamm eine Durchschnittsleistung von 100 W und eine Pulsdauer von 230 fs vorweist. Des Weiteren wurde nachgewiesen, dass der CPA, das geringe Phasenrauschen des Seed-Lasers im Bereich unter 100 kHz erhaltet und darüber hinaus, geringeres Intensitätsrauschen als vergleichbare Lasersysteme vorweist. Deshalb stellt das System eine ideale Lichtquelle für die Aufgabe Präzisionsspektroskopie dar.